Available online at www.sciencedirect.com

SCIENCE DIRECT®

Lithos 86 (2006) 50–76

LITHOS

www.elsevier.com/locate/lithos

Geochemical constraints on the Cenozoic, OIB-type alkaline volcanic rocks of NW Turkey: Implications for mantle sources and melting processes

E. Aldanmaz[a,*], N. Köprübaşı[a], Ö.F. Gürer[a], N. Kaymakçı[b], A. Gourgaud[c]

[a]*Department of Geology, University of Kocaeli, Izmit 41040, Turkey*
[b]*Department of Geology, Middle East Technical University, Ankara 06531, Turkey*
[c]*Universite Blaise Pascal, Department de Geologie, CNRS-UMR 6524, OPGS, CRV, 5 rue Kessler, Clermont-Ferrand Cedex, 63038, France*

Received 19 April 2004; accepted 15 April 2005
Available online 13 June 2005

Abstract

The volcanic province of North-West Turkey contains a number of intra-continental alkaline volcanic eruption sequences formed along the localized extensional basins developed in relation with the Late Cenozoic extensional processes. The volcanic suite comprises the extracted melt products of adiabatic decompression melting of the mantle that are represented by small-volume intra-continental plate volcanic rocks of alkaline olivine basalts and basanites with compositions representative of mantle-derived, primary (or near-primary) melts. The volcanic rocks have near-uniform $^{87}Sr/^{86}Sr$ (0.70316–70353) and $^{143}Nd/^{144}Nd$ (0.51291–0.51297; $\varepsilon_{Nd}=5.08$–6.32) ratios and are characterized by Ocean Island Basalt (OIB)-type trace element patterns with significant enrichment in LILE, HFSE and L-MREE, and a slight depletion in HREE, relative to N-MORB. Trace element variations of individual basaltic eruption sequences indicate that each lava sequence shows remarkably similar temporal–compositional trends that are characterized by an increase in incompatible elements and MgO, with decreasing SiO_2, as melt production proceeds. Systematic change in incompatible trace element concentrations (and ratios) of the lavas is not reflected by the isotopic ratios, leading to the suggestion that the temporal–compositional trends are not caused by source variations. The variations in melt chemistry with time does not reflect fractional crystallization nor can it be explained by variable proportions of mixing between melts produced by different degrees of partial melting of two (or more) compositionally distinct sources in the mantle. Instead, the observed trends are consistent with a progressive decrease in degree of melting from early-formed alkali olivine basalts to later basanites and systematic mixing between increments of melt derived from the same source but probably at different depths. Quantitative trace element modeling of fractionation-corrected data indicates that the mafic alkaline magmas originated from mixing of melts produced by variable degrees (~2% to 8%) of incremental partial melting of a compositionally uniform, volatile-bearing mantle domain

* Corresponding author.
E-mail address: ercan.aldanmaz@dunelm.org.uk (E. Aldanmaz).

0024-4937/$ - see front matter
doi:10.1016/j.lithos.2005.04.003

that is enriched in all incompatible elements (e.g. LILE, HFSE and L-MREE) relative to hypothetical Depleted MORB Mantle (DMM) and/or Primitive Mantle (PM) compositions.

Keywords: Intra-plate basalts; OIB genesis; Mantle melting; Melt metasomatism; Melt/solid reaction; Trace element modeling; Radiogenic isotopes

1. Introduction

Isentropic decompression melting linked to either actively upwelling mantle plumes or convectively upwelling hot (and buoyant) mantle materials is widely believed to be responsible for the genesis of considerable volume of primary basaltic magma that constitute mafic volcanic suites of oceanic islands and intra-continental extensional settings (e.g., McKenzie and Bickle, 1988; White and McKenzie, 1989). A large number of recent works have alternatively linked the origin of small volumes of primary melts to direct melting of thermally perturbed mantle lithosphere and developed models of melt generation from chemically distinct parts of mantle domains. The melt products of adiabatic decompression melting in the upper mantle preserve information on the composition of the mantle, the depth range over which melting takes place, and the mechanisms and extents of melt extraction. Particularly, if primary melts travel from their mantle sources to the surface without significant contamination and crystallization en route, compositional variations within them may provide direct information about the nature of the mantle sources and the array of processes that led to generation and eruption of the melts.

In western Turkey, widespread calc-alkaline volcanic activity was followed by volumetrically minor, late-stage alkaline volcanism during the Late Miocene–Quaternary, which produced a series of scattered outcrops of silica-undersaturated mafic lava flows along the localized extensional zones (Fig. 1). The genetic link between the formation of the Cenozoic magmatism and the regional tectonic evolution has been the subject of a considerable number of recent studies. The main conclusion of these studies is that the formation of the alkaline magmatism in a collisional setting of western Turkey is related to the late-stage extension developed as a consequence of a late post-collisional stage of relaxation and extensional faulting, following an early plate convergence and collision (e.g. Aldanmaz et al., 2000, and references therein). The characteristics of the mantle source and melt generation processes, however, remain to be constrained.

Conclusions of earlier works carried out to place constraints on the processes of melt generation to produce the alkaline magmas in western Turkey vary significantly. Some investigators have attempted to explain the generation of alkaline magma by proposing a mixing of melts from discrete mantle components, a model also largely invoked to explain the formation of many OIB-type (both oceanic and continental) alkaline settings elsewhere. McKenzie and O'Nions (1995), for instance, used REE data to propose that the extensional mafic volcanic rocks of western Turkey were derived from melts generated within mantle lithosphere that had previously been enriched by melt fractions from the mantle asthenosphere. They suggested that estimated extension rates across the area are probably too small (β factors < 1.2; Paton, 1992) to explain dry melting of convective mantle without added effect of elevated temperatures (e.g. a mantle plume). A somewhat similar conclusion was later introduced by Alıcı et al. (2002) who, based on trace element and isotope data, proposed a mixing of melts from both lithospheric and asthenospheric sources for the origin of Quaternary alkaline lavas of western Turkey. Aldanmaz et al. (2000), on the other hand, used trace element and isotope data to demonstrate the improbability of involvement of a mantle lithospheric source. They proposed a homogeneous convecting mantle as the source for the alkaline magmas.

In this contribution we examine the primitive alkaline volcanic rocks from the Cenozoic volcanic province of NW Turkey and report a new temporally-controlled geochemical data set for the lava sequences. The province provides a clear opportunity for study of the processes of mantle melting and melt

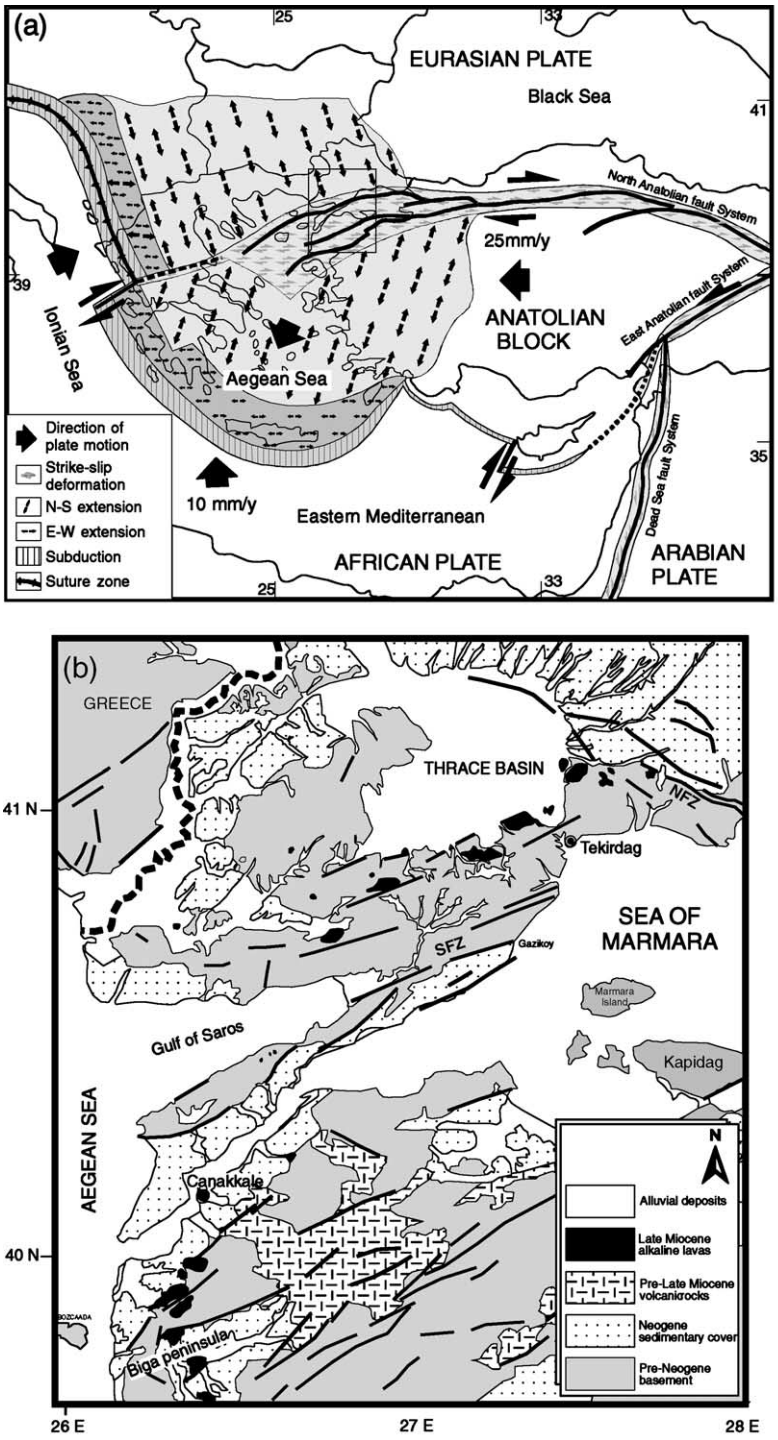

Fig. 1. (a) Map showing the plate reconstruction of eastern Mediterranean. (b) Simplified geological map of NW Turkey showing the distribution of the alkaline volcanic products and the main eruption centers.

migration in upwelling upper mantle. The erupted basalts are relatively free of the complicating effects of mantle lithosphere or crustal interactions and several of these lavas have bulk compositions that may approximate primary melts. Chemical data from these rocks may, thus, provide essential evidence that constrains the nature of the melting and melt extraction processes and the characteristics of the mantle source. We particularly focus on modeling and interpreting trace element and Sr–Nd isotopic data, with a special emphasis of providing insights into: (1) the characteristics of the mantle source of the alkaline magma(s) in terms of chemical composition; (2) the primary controls on melt generation and processes of melt migration; and (3) the possible effects of the shallow-level processes such as fractional crystallization and crustal contamination on a mantle-derived (primary) magma(s). We also evaluate proposals calling for contributions from lithologically and chemically discrete mantle components in the genesis of ocean island basalt.

2. Geological setting and nature of volcanic rocks

The geological characteristics of NW Turkey have been described in detail in a number of recent studies (e.g. Yilmaz and Polat, 1998; Aldanmaz et al., 2000, 2005), and only a brief description will be given here. The tectonic evolution of NW Turkey has been largely influenced by collision of the African and Arabian plates with the Eurasian plate. The main collision that took place between the Anatolian and Arabian plates is assumed to cause the major shortening and uplift in eastern Turkey and the westward extrusion of the wedge-shaped Anatolian microplate as a buoyant continental sliver, which is accommodated by two major faults: the right-lateral strike-slip along the North Anatolian Fault (NAF) and the left-lateral strike-slip along the East Anatolian Fault (EAF). The effect of the major, dextral, E–W trending strike-slip activity along the NAF was that the movement of the Anatolian plate relative to the Eurasian plate changed from westward to south-westward with changing patterns of deformation from pure strike-slip along its eastern and central segments into a combination of right lateral and extensional mechanisms along the western segment (Fig. 1). This led to a right-lateral transtensional tectonics, generating small pull-apart basins related to NE–SW trending strike-slip faulting in NW Turkey (e.g. in the Biga Peninsula and the Thrace basin; Fig. 1) during the Late Miocene onward.

In the Biga Peninsula, the alkaline volcanic field comprises a number of sub-horizontal lava flows lying on the localized extensional basins. The rocks in this area are mainly fine-grained olivine-phyric or aphyric basalts and basanites. The published radiometric dates (K–Ar and Ar–Ar) reveal that the alkaline volcanic activity lasted from 11.16 ± 0.21 to 7.65 ± 0.36 Ma (Aldanmaz et al., 2000; Kaymakçi et al., submitted for publication). Characteristics of volcanic rocks from the central and southern parts of the peninsula have been reported previously (e.g. Aldanmaz et al., 2000; Aldanmaz, 2002). In this contribution, we will focus on alkaline volcanic rocks from the northernmost part of the peninsula (from Çanakkale) as one of two most voluminous alkaline volcanic suites of NW Turkey.

Further north, in the Thrace basin, small isolated lava flows attain a maximum thickness of 100 m. The alkaline volcanic field lies along the southern margin of the triangle-shaped Thrace basin as the eruption centers are linearly distributed along the margin and are aligned approximately NW–SE direction within a shear zone delimited by a number of strike-slip faults (Fig. 1). The available radiometric dates (11.68 ± 0.25 to 6.47 ± 0.47 Ma; Paton, 1992; Kaymakçi et al., submitted for publication) yield an Upper Miocene age for the alkaline volcanic rocks of the Thrace region. The rocks from the Thrace volcanic field are compositionally identical to those from Çanakkale and are likely originated from the same source. Unlike the Çanakkale suite, however, the Thrace lavas are generally less phyric and contain large amounts of mantle-derived peridotite xenoliths.

The rocks from both suits are petrographically similar to one another. The samples are extremely fresh with only a few showing incipient alteration of olivine phenocrysts along rims and interior cracks upon microscopic investigations. They consist of a fine-grained matrix with small to medium-sized (<5 mm) phenocrysts of olivine and rare clinopyroxene. Phenocryst contents are variable, generally ranging from <3% (aphyric) to 15% (weakly porphyritic), but the majority of the rocks are aphyric. The olivine phenocrysts are commonly subhedral and their abundances range between 40% and 70% of the total

Table 1
Whole-rock major and trace element data for the volcanic rock samples from NW Turkey

Locality	Thrace	Thrace	Thrace	Thrace	Thrace	Thrace	Thrace	Thrace	Thrace	Thrace	Thrace	Thrace	Thrace	Thrace	Thrace	C.kale	C.kale	C.kale	C.kale	C.kale
Sample no	EA517	EA516	EA520	EA509	EA513	EA521	EA514	EA519	EA522	EA510	EA508	EA518	EA515	EA511	EA512	EA531	EA534	EA258	EA259	EA260
Rock type	Basanite	Basanite	Basanite	Alk-bas	Alk-bas	Basanite	Basanite	Basanite	Basanite	Alk-bas	Basanite	Alk-bas	Basanite	Alk-bas	Alk-bas	Basanite	Basanite	Basanite	Basanite	Basanite
SiO_2	43.74	43.63	43.51	45.12	45.97	43.36	44.17	43.27	44.85	45.25	44.82	45.98	43.99	47.83	47.91	42.66	42.88	44.33	44.84	42.75
TiO_2	2.67	2.63	2.59	2.71	2.97	2.61	2.61	2.60	2.70	2.79	2.70	2.79	2.60	2.70	2.71	3.22	3.23	3.04	2.98	3.09
Al_2O_3	11.74	11.62	12.65	12.24	13.09	12.78	12.23	12.67	12.55	12.80	12.27	14.52	11.68	13.53	13.74	13.44	13.32	12.49	13.01	12.87
Fe_2O_3	10.84	10.82	11.31	10.59	12.50	11.36	10.59	11.29	10.38	10.35	10.68	10.99	10.91	10.69	10.53	13.19	13.08	14.07	13.62	14.30
MnO	0.16	0.16	0.16	0.15	0.17	0.17	0.16	0.16	0.15	0.15	0.15	0.15	0.16	0.16	0.15	0.21	0.21	0.20	0.20	0.21
MgO	12.89	13.48	10.31	11.61	8.45	10.62	12.54	9.81	11.29	10.48	11.44	7.08	13.37	7.22	6.79	7.17	7.17	8.33	7.52	8.19
CaO	9.19	9.12	10.74	9.04	10.16	10.44	8.90	10.71	8.86	8.79	8.85	10.44	8.89	9.30	9.97	10.73	10.74	10.94	10.91	10.91
Na_2O	3.43	3.33	3.13	3.05	3.51	3.09	3.49	3.03	2.61	3.32	3.19	2.66	3.44	3.89	3.87	4.65	4.56	4.22	4.34	4.33
K_2O	1.27	1.33	0.85	1.56	1.52	0.82	2.04	0.78	1.25	1.97	1.61	1.84	2.12	1.55	1.61	1.58	1.55	1.23	1.46	1.42
P_2O_5	0.90	0.88	0.71	0.69	0.69	0.67	0.83	0.68	0.71	0.77	0.69	0.58	0.76	0.58	0.58	1.09	1.12	1.09	1.08	0.99
L.O.I	3.20	2.80	3.80	3.10	0.80	3.90	2.30	4.70	4.50	3.20	3.40	2.80	1.90	2.40	2.10	1.70	1.90	1.83	1.30	1.57
Total	99.97	99.96	99.86	99.98	99.94	100.01	99.97	99.80	99.97	99.98	99.97	99.92	99.98	99.95	99.95	99.83	99.84	99.94	99.96	99.07
Sc	17.0	17.3	25.5	19.7	21.3	25.6	18.4	25.3	18.9	18.5	20.1	22.0	19.4	20.3	20.1	18.0	18.0	19.7	19.2	16.9
Cr	410.5	444.7	253.2	376.3	301.0	225.8	431.0	246.3	369.5	390.0	622.6	225.8	533.7	335.3	287.4	205.3	116.3	138.1	134.7	137.3
V	172.5	167.3	191.9	164.2	187.4	207.2	163.0	202.5	181.3	161.6	159.4	208.3	170.1	176.8	170.3	217.3	212.4	204.5	203.7	211.3
Ni	332.7	363.6	151.2	256.8	140.2	144.2	319.3	145.9	262.7	217.0	278.3	59.1	346.5	126.1	109.4	61.0	66.1	99.6	95.4	104.5
Co	55.2	54.2	50.0	48.6	49.0	51.9	50.5	51.8	50.2	45.5	49.6	40.5	54.4	44.2	40.5	48.0	46.7	49.0	48.1	50.9
Cu	40.8	38.2	61.1	43.8	48.7	60.2	46.4	61.6	39.8	46.2	55.0	59.0	43.3	27.7	27.9	46.4	44.8	40.6	43.1	43.3
Zn	76.7	70.3	79.2	71.8	99.0	77.6	75.4	79.1	70.3	68.4	77.2	89.6	72.4	59.3	54.0	115.3	113.7	127.9	128.6	120.7
Ga	20.2	20.5	20.7	17.7	21.2	21.5	19.3	21.5	21.8	19.2	18.4	22.7	19.7	21.3	20.2	27.9	25.0	19.6	21.1	23.2
Rb	36.5	39.4	11.9	22.4	19.7	9.5	22.7	11.0	9.9	24.9	20.2	25.8	19.9	13.3	11.1	42.3	41.4	19.3	18.5	17.3
Sr	959.5	979.5	803.9	734.5	675.2	841.8	838.2	837.1	872.6	745.9	725.3	1222.0	759.6	711.6	783.6	1056.2	1047.8	1005.7	951.3	908.3
Y	23.7	22.7	22.8	21.1	26.9	23.1	20.6	22.8	22.3	21.3	20.3	23.1	21.4	22.9	22.0	34.8	33.1	32.3	33.5	31.5
Zr	253.1	251.1	221.7	216.4	215.9	217.1	217.1	215.2	215.3	214.5	197.3	181.3	176.8	171.8	162.9	324.1	321.7	317.3	308.7	264.1
Nb	88.7	87.2	74.8	73.2	72.7	72.1	74.1	72.4	71.3	70.7	64.0	57.4	57.1	52.3	47.8	98.7	97.7	95.8	91.4	74.4
Cs	0.8	0.7	0.7	0.4	0.5	0.7	0.6	0.6	0.6	0.5	0.6	0.3	0.6	0.8	0.7	0.8	1.0	0.7	0.6	0.5
Ba	456.4	445.1	491.3	332.9	407.5	493.0	418.3	525.7	341.8	348.3	337.0	418.2	386.6	299.4	300.7	759.5	502.3	602.1	596.6	511.5
La	36.27	35.75	32.52	31.78	31.71	31.49	31.22	31.14	30.13	29.76	28.19	25.42	25.16	23.95	23.24	63.37	62.13	61.60	58.60	54.65

Ce	75.54	75.04	67.94	67.24	66.37	66.85	66.15	64.90	63.60	61.10	60.23	54.36	53.26	50.53	48.72	120.53	118.68	117.35	114.86	107.47
Pr	9.16	9.07	8.18	8.25	8.02	8.06	8.02	8.02	7.84	7.51	7.42	6.60	6.52	6.27	5.96	14.24	14.17	13.94	13.33	12.72
Nd	39.89	39.51	35.29	35.43	34.73	35.12	34.36	34.21	33.42	32.27	32.01	28.47	28.35	27.11	25.98	59.93	59.17	57.81	55.86	54.14
Sm	8.21	8.11	7.58	7.58	7.49	7.41	7.35	7.46	7.19	7.12	6.98	6.49	6.42	6.37	6.20	11.35	11.34	11.12	10.77	10.51
Eu	2.61	2.56	2.39	2.41	2.38	2.39	2.31	2.38	2.28	2.28	2.21	2.06	2.03	2.01	1.96	3.40	3.39	3.43	3.22	3.20
Gd	7.42	7.25	6.94	6.98	6.87	6.88	6.69	6.91	6.55	6.42	6.45	5.98	5.87	5.93	5.68	9.21	9.31	9.37	9.27	8.89
Tb	1.02	1.01	0.97	0.97	0.96	0.97	0.93	0.96	0.94	0.91	0.91	0.83	0.82	0.83	0.80	1.36	1.35	1.33	1.31	1.30
Dy	5.24	5.15	5.01	5.01	4.99	4.98	4.81	4.99	4.88	4.69	4.72	4.39	4.28	4.22	4.06	6.79	6.70	6.73	6.56	6.46
Ho	0.91	0.90	0.88	0.88	0.88	0.87	0.85	0.86	0.86	0.83	0.83	0.77	0.76	0.75	0.74	1.19	1.19	1.18	1.14	1.12
Er	2.08	2.05	1.98	2.02	2.04	2.00	1.92	1.98	1.95	1.89	1.91	1.81	1.80	1.72	1.71	2.91	2.81	2.78	2.79	2.62
Tm	0.25	0.26	0.25	0.25	0.25	0.25	0.24	0.25	0.24	0.24	0.24	0.23	0.23	0.23	0.23	0.41	0.40	0.40	0.40	0.38
Yb	1.49	1.47	1.43	1.43	1.42	1.42	1.40	1.41	1.39	1.39	1.37	1.32	1.32	1.31	1.30	2.26	2.20	2.22	2.15	2.07
Lu	0.20	0.20	0.20	0.19	0.19	0.19	0.19	0.19	0.19	0.19	0.18	0.18	0.17	0.17	0.17	0.31	0.30	0.30	0.29	0.28
Hf	5.49	5.31	5.06	4.88	4.98	4.84	5.15	4.97	4.92	4.94	4.72	4.52	4.61	4.28	4.23	7.47	7.34	7.38	7.21	6.99
Ta	5.05	4.98	4.38	4.31	4.23	4.26	4.32	4.22	4.11	4.01	3.71	3.33	3.30	2.98	2.89	6.23	6.03	5.93	5.65	5.54
Pb	2.90	2.70	1.60	1.90	2.10	1.70	2.40	1.80	1.00	1.70	2.70	1.50	2.20	0.40	0.50	3.30	3.10	6.83	6.54	5.73
Th	6.26	6.20	5.28	5.13	4.98	4.99	4.97	4.87	4.75	4.69	4.27	3.66	3.61	3.12	2.96	8.16	7.93	8.01	7.56	7.22
U	2.21	2.06	1.60	1.37	1.63	1.40	1.51	1.33	1.60	1.50	1.28	1.07	1.24	0.87	0.98	3.20	2.60	3.11	2.98	2.32
Fractionation corrected values																				
La	36.27	35.75	32.52	31.78	26.10	31.49	31.22	28.08	30.13	29.76	28.19	20.42	25.16	19.71	18.67	44.66	44.40	46.46	41.88	40.14
Ce	75.54	75.04	67.94	67.24	54.80	66.85	66.15	58.62	63.60	61.10	60.23	43.83	53.26	41.72	39.28	85.42	85.27	88.90	82.52	79.31
Nd	39.89	39.51	35.29	35.57	28.90	35.12	34.36	31.09	33.42	32.27	32.13	23.16	28.44	22.59	21.13	43.15	43.09	44.29	40.68	40.46
Zr	253.10	251.10	221.70	216.40	178.50	217.10	217.10	194.53	215.30	214.50	197.30	146.39	176.80	142.04	131.53	230.25	231.68	240.83	222.31	195.33
Nb	88.70	87.20	74.80	73.20	59.74	72.10	74.10	65.23	71.30	70.70	64.00	46.03	57.10	42.97	38.33	69.36	69.63	72.06	65.12	54.49
Ta	5.05	4.98	4.38	4.31	3.48	4.26	4.32	3.80	4.11	4.01	3.71	2.67	3.30	2.45	2.32	4.38	4.30	4.46	4.03	4.06
Yb	1.49	1.47	1.43	1.43	1.19	1.42	1.40	1.28	1.39	1.39	1.37	1.08	1.32	1.10	1.06	1.64	1.62	1.71	1.58	1.56
Th	6.26	6.20	5.28	5.13	4.08	4.99	4.97	4.38	4.75	4.69	4.27	2.93	3.61	2.56	2.37	5.71	5.63	6.01	5.37	5.27

Primary melt compositions were calculated by adding mineral phases, which are presumed to have fractionated during magma ascent, back into the magma. The proportion of mineral phases for each sample was approximated using their modal abundances.

Table 1 (*continued*)

Locality	C.kale	C.kale	C.kale	C.kale	C.kale	C.kale	C.kale	C.kale	C.kale	C.kale	C.kale	C.kale	C.kale	C.kale	C.kale	C.kale	C.kale	C.kale	C.kale	C.kale	C.kale
Sample no	EA252	EA533	EA528	EA254	EA527	EA529	EA415	EA262	EA261	EA242	EA264	EA526	EA247	EA525	EA523	EA524	EA255	EA532	EA249	EA251	EA530
Rock type	Alk-bas	Basanite	Basanite	Alk-bas	Basanite	Basanite	Alk-bas	Alk-bas	Alk-bas	Alk-bas	Alk-bas	Alk-bas	Alk-bas	Alk-bas	Alk-bas	Alk-bas	Alk-bas	Alk-bas	Alk-bas	Alk-bas	Alk-bas
SiO_2	45.68	44.82	44.95	45.69	44.69	44.57	46.07	46.99	45.88	46.39	46.87	45.79	47.17	46.74	46.68	46.06	50.34	48.77	49.97	50.13	48.73
TiO_2	2.83	2.91	2.97	2.78	2.97	2.93	2.83	2.82	2.78	2.84	2.85	2.95	2.56	2.75	2.74	2.71	2.62	2.84	2.58	2.58	2.82
Al_2O_3	13.38	13.29	13.48	13.29	13.47	13.33	13.21	13.01	12.87	12.87	13.08	13.11	13.19	13.51	13.46	13.27	14.67	14.43	14.30	14.65	14.53
Fe_2O_3	12.19	11.55	11.82	12.13	11.74	11.68	12.04	12.22	12.43	12.21	12.28	12.28	11.16	11.02	11.13	11.12	10.78	10.32	10.69	10.66	10.44
MnO	0.17	0.16	0.17	0.17	0.17	0.17	0.16	0.18	0.21	0.17	0.15	0.18	0.15	0.15	0.15	0.16	0.12	0.12	0.14	0.14	0.14
MgO	9.48	8.74	8.88	9.62	9.02	9.15	9.25	8.38	8.43	8.47	7.72	8.39	8.25	8.21	8.78	8.69	6.59	6.11	6.90	6.54	6.44
CaO	10.35	10.24	10.09	9.96	10.06	10.02	10.91	10.76	11.79	9.83	11.64	9.86	9.95	9.77	9.42	9.91	8.98	9.18	8.74	9.43	8.97
Na_2O	3.78	2.72	3.67	4.25	3.76	3.58	3.14	3.49	3.47	3.02	3.19	2.83	2.98	3.26	2.91	2.82	3.68	3.17	3.51	3.65	3.05
K_2O	1.52	1.58	1.62	1.57	1.58	1.48	1.51	1.67	1.62	1.57	1.68	1.44	1.61	1.57	1.59	1.65	1.64	1.59	1.63	1.62	1.56
P_2O_5	0.82	0.78	0.82	0.79	0.80	0.84	0.76	0.74	0.73	0.72	0.71	0.69	0.62	0.63	0.62	0.62	0.50	0.51	0.49	0.49	0.51
L.O.I	2.08	2.80	1.40	1.27	2.20	2.10	2.83	1.86	2.94	1.37	2.66	2.20	1.89	2.70	2.40	2.90	1.79	2.80	1.46	1.65	2.70
Total	100.19	99.70	99.97	100.25	99.95	99.94	99.88	100.25	100.21	98.09	100.17	99.94	97.64	99.98	99.97	99.96	99.92	99.89	98.95	99.89	99.97
Sc	22.9	20.0	21.0	19.0	20.0	21.0	18.5	18.9	16.8	18.4	23.2	20.0	20.0	20.0	20.0	20.0	22.5	19.0	20.1	21.8	19.0
Cr	190.3	266.8	239.5	194.6	225.8	212.1	228.5	239.2	229.0	227.9	228.4	232.6	301.2	266.8	328.4	273.7	213.6	218.9	278.6	217.8	246.3
V	192.0	210.7	200.1	200.8	198.6	196.4	208.5	203.2	196.4	186.1	209.1	205.8	210.4	194.2	190.8	189.3	200.5	198.2	200.4	203.9	187.5
Ni	146.4	129.9	133.8	142.3	127.3	123.7	168.6	156.0	149.0	153.7	163.0	136.8	157.8	155.5	162.2	160.2	153.7	61.8	176.9	174.6	61.0
Co	50.1	48.7	49.9	47.9	49.0	48.2	47.7	46.8	41.9	43.8	48.3	51.2	45.2	47.2	46.0	46.1	38.2	39.6	35.4	36.8	37.6
Cu	52.2	45.5	46.2	47.6	51.2	45.3	43.5	52.7	47.7	49.0	54.3	44.9	51.9	37.6	42.9	64.8	35.1	47.8	13.3	33.5	43.7
Zn	100.8	44.6	98.2	107.0	80.4	94.8	99.2	108.4	105.2	103.5	105.0	100.5	102.1	89.1	93.6	95.4	101.5	58.6	95.5	96.8	73.0
Ga	24.1	24.1	24.1	22.7	22.5	23.1	21.3	21.4	20.1	21.3	18.6	22.6	20.4	22.8	21.5	19.8	17.9	23.6	20.6	14.8	23.2
Rb	16.9	23.0	21.1	16.5	13.5	15.4	24.1	21.7	21.6	19.0	18.4	18.4	26.0	14.9	21.4	17.0	20.1	18.5	17.9	18.6	17.7
Sr	792.7	1065.2	814.2	815.7	882.7	851.6	728.6	788.6	751.2	739.7	643.0	1126.8	623.1	683.0	619.7	626.8	594.6	614.4	505.9	556.2	545.9
Y	25.9	26.8	27.5	27.7	27.1	26.6	25.8	27.3	24.4	26.3	24.7	28.3	23.5	24.3	23.5	23.2	23.3	22.2	21.3	20.8	21.8
Zr	259.0	244.4	241.1	247.3	237.0	239.5	246.5	244.9	240.1	239.6	231.4	219.7	216.2	214.4	205.9	196.1	189.0	187.6	185.3	187.4	181.1
Nb	71.8	64.8	65.4	69.0	63.7	63.3	65.7	65.0	65.0	62.8	59.4	56.6	55.1	52.3	48.9	44.9	43.9	41.2	40.4	43.3	37.7
Cs	0.4	1.1	2.1	1.1	1.1	1.2	1.2	0.8	0.8	0.7	0.6	0.3	1.2	1.1	1.9	1.3	1.5	1.5	1.7	1.9	1.1
Ba	456.6	563.7	402.7	455.8	391.3	388.2	418.6	469.5	410.9	399.8	370.0	311.9	352.9	332.6	322.0	351.3	267.3	274.2	245.0	253.6	248.6
La	42.11	40.65	39.04	38.68	38.18	37.76	37.26	36.92	36.73	36.60	34.27	33.68	29.90	29.54	29.23	27.57	22.17	21.92	20.00	20.56	19.91

Ce	82.66	81.73	79.15	79.27	79.13	77.02	74.02	73.49	74.80	72.56	68.30	69.05	62.29	61.81	61.32	57.53	48.13	45.83	42.86	42.19	41.35
Pr	10.00	10.06	9.73	9.34	9.77	9.52	8.79	8.98	8.91	8.89	8.42	8.69	7.53	7.82	7.71	7.16	5.97	5.84	5.57	5.65	5.29
Nd	42.49	42.11	42.13	39.59	42.31	41.13	39.10	39.79	38.13	38.02	36.13	37.56	31.79	33.51	32.86	30.68	26.32	25.97	25.36	25.02	22.94
Sm	8.67	8.62	8.51	8.29	8.44	8.51	8.08	8.13	8.19	8.02	7.71	7.82	7.29	7.61	7.35	7.02	6.37	6.54	6.01	6.13	5.80
Eu	2.76	2.79	2.73	2.57	2.78	2.78	2.52	2.56	2.50	2.47	2.49	2.56	2.23	2.39	2.38	2.19	2.02	2.02	1.94	1.99	1.82
Gd	7.54	7.68	7.66	7.39	7.88	7.72	7.31	7.08	7.38	7.07	6.87	7.36	6.79	6.82	6.71	6.27	5.72	5.88	5.85	5.88	5.35
Tb	1.12	1.11	1.08	1.09	1.10	1.09	1.06	1.07	1.09	1.06	1.03	1.07	0.97	1.03	1.01	0.91	0.88	0.87	0.85	0.86	0.78
Dy	5.77	5.63	5.71	5.46	5.71	5.53	5.33	5.52	5.30	5.33	5.31	5.43	4.95	5.11	5.18	4.76	4.44	4.48	4.35	4.47	4.03
Ho	0.98	0.98	0.96	0.97	0.96	0.95	0.93	0.98	0.93	0.94	0.91	0.93	0.86	0.91	0.90	0.84	0.78	0.80	0.77	0.79	0.73
Er	2.26	2.32	2.31	2.23	2.29	2.27	2.16	2.21	2.28	2.21	2.05	2.09	2.02	2.09	2.05	1.93	1.84	1.85	1.78	1.81	1.69
Tm	0.33	0.32	0.31	0.32	0.31	0.31	0.32	0.32	0.31	0.31	0.30	0.31	0.29	0.28	0.28	0.27	0.26	0.25	0.25	0.25	0.23
Yb	1.81	1.82	1.83	1.83	1.82	1.72	1.71	1.79	1.71	1.79	1.67	1.74	1.69	1.65	1.63	1.56	1.54	1.50	1.47	1.45	1.43
Lu	0.25	0.25	0.25	0.25	0.25	0.24	0.24	0.25	0.24	0.25	0.23	0.24	0.24	0.23	0.23	0.22	0.22	0.21	0.21	0.21	0.20
Hf	5.93	5.89	5.88	5.88	5.84	5.88	5.52	5.57	5.46	5.59	5.31	5.33	5.19	5.16	5.11	4.92	4.45	4.43	4.34	4.34	4.35
Ta	4.34	4.28	4.12	4.06	4.04	3.98	3.97	3.79	3.64	3.63	3.46	3.54	3.13	3.28	3.11	3.12	2.39	2.41	2.18	2.24	2.43
Pb	5.06	0.40	1.60	4.91	1.10	0.90	4.62	4.33	5.12	3.73	4.17	1.80	3.65	1.00	1.20	1.50	3.92	1.30	2.03	3.96	1.10
Th	5.53	5.29	5.25	5.24	5.11	5.18	5.01	4.77	4.83	4.72	4.42	4.27	3.95	3.91	3.83	3.71	2.88	2.69	2.53	2.65	2.75
U	2.23	1.70	1.90	1.90	1.80	1.50	1.13	1.61	1.98	1.98	1.87	1.20	1.67	1.40	1.20	1.60	1.32	0.90	1.10	1.25	0.90
Fractionation corrected values																					
La	36.73	35.06	33.67	34.13	33.31	32.94	32.14	30.75	30.23	25.07	26.86	27.72	25.49	25.19	25.50	24.05	17.16	16.53	16.07	15.91	15.41
Ce	72.26	70.66	68.43	70.07	69.18	67.33	63.99	61.40	61.76	50.01	53.73	57.01	53.25	52.83	53.61	50.29	37.40	34.72	34.55	32.78	32.13
Nd	37.35	36.62	36.64	35.17	37.13	36.15	34.01	33.48	31.73	26.60	28.71	31.41	27.35	28.83	28.99	26.97	20.66	19.90	20.63	19.64	18.01
Zr	226.61	211.50	208.65	218.78	207.39	209.57	213.36	204.84	198.51	165.59	182.36	181.64	184.97	183.47	180.17	171.60	147.12	142.39	149.60	145.87	140.97
Nb	62.56	55.81	56.33	60.80	55.50	55.15	56.58	54.06	53.43	42.87	46.48	46.51	46.95	44.53	42.61	39.08	33.91	30.99	32.38	33.40	29.08
Ta	3.78	3.69	3.55	3.58	3.52	3.47	3.42	3.15	2.99	2.48	2.71	2.91	2.66	2.79	2.71	2.72	1.85	1.81	1.75	1.73	1.88
Yb	1.60	1.59	1.60	1.63	1.61	1.52	1.50	1.51	1.43	1.26	1.34	1.46	1.46	1.43	1.44	1.38	1.22	1.16	1.20	1.15	1.13
Th	4.81	4.55	4.52	4.61	4.45	4.51	4.31	3.96	3.96	3.21	3.45	3.50	3.36	3.32	3.33	3.23	2.22	2.02	2.02	2.04	2.12

phenocrysts. No significant compositional zoning has been observed; core and rim compositions are $Fo_{73–92}$ and $Fo_{71–91}$ respectively. Clinopyroxene phenocrysts ($Wo_{43–49}$), when they exist, display glomerophyric textures due to clustered clinopyroxene crystals radiating outward from early-formed olivine crystals. Plagioclase does not occur as a phenocryst phase, but some samples contain plagioclase laths in their microcrystalline groundmass ($An_{77–95}$). Ilmenite (90% to 98% ilmenite) and magnetite (28% to 87% ulvöspinel) form euhedral and subhedral microcrysts that range from ~1 to 0.05 mm.

3. Analytical procedures

We have analyzed a total of forty-one volcanic rocks for major and trace elements. Rock powders were prepared by removing the xenoliths and altered surfaces, crushing and then grinding in an agate ball mill. Major and selected trace element abundances of a total of twenty four volcanic rock samples from both the Çanakkale and Thrace volcanic areas were measured on fused discs and pressed powder pellets respectively, using an automated Philips PW1400 XRF spectrometer with a rhodium anode tube at the University of Durham. Loss on ignition (LOI) was determined by heating a separate aliquot of rock powder at 900 °C for >2 h. The same samples were dissolved and analyzed by ICP–MS at the University of Durham (UK) for a total of 36 minor and trace elements.

In addition, seventeen samples were analyzed at the ACME analytical laboratories at Vancouver. Rock powders were fused and then dissolved to prepare the solutions from which the major and trace element abundances were determined using ICP–AES and ICP–MS respectively. Whole rock major and trace element data for alkaline volcanic rocks are given in Table 1.

Radiogenic isotope ratios for Sr and Nd were determined at the University of Clermont-Ferrand (France). The analytical techniques used for the separation of Sr and Nd have been reported by Pin et al. (1994). Sr was loaded onto a single Ta filament whereas Nd was loaded onto a triple Ta–Re–Ta assembly. Metal ions were used for the analyses. Both Sr and Nd were measured using a Micromass VG 54E mass spectrometer, in the double and triple collection modes respectively. Mass fractionation for Sr and Nd was corrected by normalizing to $^{86}Sr/^{88}Sr=0.1194$ and $^{146}Nd/^{144}Nd=0.7219$. The Sr and Nd isotope ratios are given relative to an $^{87}Sr/^{86}Sr$ of 0.710237 and a $^{143}Nd/^{144}Nd$ of 0.511975 for the NBS 987 and AMES standards, respectively.

Mineral analyses from the volcanic rocks were performed using a Cameca CAMEBAX electron microprobe at the Université Blaise Pascal (France) with operating conditions of 15 kV accelerating voltage, 10–12 nA beam current and 10 s counting time per element.

4. Major and trace element chemistry

The lavas from both Çanakkale and the Thrace volcanic field are a strongly alkaline series of volcanic rocks, with almost all samples plotting in the basanite, alkali basalt and trachybasalt fields on a total alkalis (K_2O+Na_2O) vs. silica (SiO_2) classification diagram of Le Bas et al. (1986) (Fig. 2). The rocks are silica-undersaturated (nepheline-normative), sodic ($Na_2O/K_2O=1.45–3.88$) and possess high Mg# [cation proportion of $Mg/(Mg+Fe_{total})$] and high MgO (6.11–13.48 wt.%) over a range of SiO_2 content from 42.6 to 50.3 wt.%. The more magnesian samples have Mg#>0.70, are saturated with olivine in the range of Fo_{89} to Fo_{92}, and could be assessed as being in equilibrium with mantle olivine. The analyzed sam-

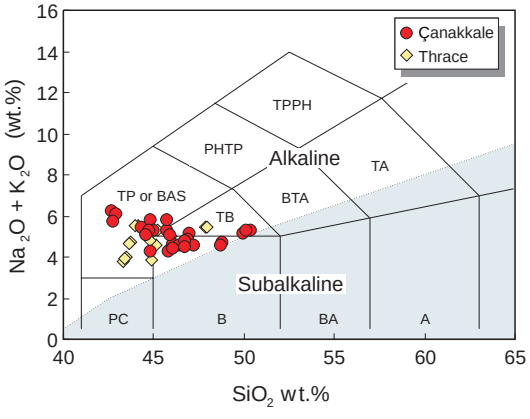

Fig. 2. Classification of the alkaline volcanic rocks from western Anatolia on a TAS diagram of Le Bas et al. (1986). Key to abbreviations: B — basalt; TB — trachybasalt; BS — basanite.

ples have moderate Ca (8.74–11.79 wt.% CaO) and high Al (11.62–14.67 wt.% Al_2O_3) contents and their Cr and Ni concentrations range variably from 116.3 to 622.6 ppm and from 59.1 to 363.6 ppm, respectively. Although rock types and whole-rock chemical compositions show that the samples from the two suites are remarkably similar to one another, the lavas from the Thrace alkaline field are marked by their greater Mg# and Cr–Ni contents relative to those from Çanakkale, indicating that they are closer to primary melt compositions.

The alkaline rocks have almost straight and subparallel chondrite (CI)-normalized REE pattern with near-constant concentration ratios. The absolute REE abundances decrease with increasing SiO_2 content both within each phase, and through the overall eruptive sequences (Fig. 3a). All samples have LREE enriched patterns on chondrite-normalized REE plots. The lavas also have all the classic enrichments in LILE, HFSE and L-MREE and slight depletion in HREE (e.g., relative to the average N-MORB normalizing values) that characterize basalts from intraplate continental and oceanic settings (Fig. 3b). The rocks also display prominent negative Rb, K and Ti anomalies.

There are no significant differences in trace element ratios between the primary lavas and the slightly evolved ones, indicating that differentiation has played only a minor role throughout the lava sequences. Incompatible element concentrations correlate with both silica and age; in the individual eruptive sequences almost all incompatible element concentrations increase with decreasing SiO_2 contents toward the top of the sequences. This chemical trend cannot be explained by fractional crystallization, as concentrations of compatible major elements such as Mg do not vary systematically with respect to stratigraphic height of the lavas. The largely primitive compositions of the alkaline magmas also preclude a significant role of fractional crystallization in generating the observed compositional trends. Moreover, SiO_2 is negatively correlated with the contents of incompatible elements in all sequences, the opposite of what would be expected from fractional crystallization of olivine and pyroxene. This overall chemical trend is accompanied by a shift from alkali basalts to basanites, suggesting a long-term trend of progressively lower degrees of melting through multiple eruptive episodes of the mafic alkaline suite. Thus, a large component of the variation within the lava stratigraphy has to be explained by variation in the degree of melting instead of fractional crystallization.

5. Neodymium and strontium isotope variations

Nd and Sr isotopic ratios for the volcanic rock samples are plotted on an $^{87}Sr/^{86}Sr$ vs. $^{143}Nd/^{144}Nd$ diagram in Fig. 4a. The volcanic rocks are young, with insignificant radiogenic in-growth, indicating that the isotopic compositions of the rocks represent the composition of their source regions. The rocks are characterized by low $^{87}Sr/^{86}Sr$ (0.70316–70353) and high $^{143}Nd/^{144}Nd$ (0.51291–0.51297) ratios, typical of what is usually seen in OIB-type rocks from both oceanic and continental settings. The samples display a restricted range of isotopic ratios throughout the lava sequences, indicating that the mantle source of the alkaline magmas remained isotopically homogeneous during the formation of the entire suite. The NW Turkish alkaline lavas can therefore be considered cogenetic in a broad sense referring to their derivation from a single, homogeneous mantle domain. The rocks have near-constant $^{87}Sr/^{86}Sr$ and $^{143}Nd/^{144}Nd$ ratios for a relatively large range in SiO_2 content from 42.6 to 50.3 wt.%. This could be explained by fractional crystallization from isotopically homogeneous parent magma. However, systematic change and relatively large variation in ratios of certain trace elements, such as Zr/Nb, are not reflected by variations in the isotopic ratios, reinforcing the suggestion of melt generation by variable degrees of partial melting of an isotopically homogeneous source in the mantle. The $^{87}Sr/^{86}Sr$ vs. $^{143}Nd/^{144}Nd$ diagram shows that the samples all plot within the depleted quadrant of mantle array, and extend from MORB-like compositions toward the bulk silicate Earth (BSE) (Fig. 4a).

The samples are all LREE-enriched relative to average N-MORB and BSE values, with $^{147}Sm/^{144}Nd$ values from 0.119 to 0.148, and thus plot to the left of a 4.55 Ga geochron on a $^{143}Nd/^{144}Nd$ vs. $^{147}Sm/^{144}Nd$ diagram (Fig. 4b). However, the samples have present-day $^{143}Nd/^{144}Nd$ values greater than BSE, reflecting time-integrated mantle source history of

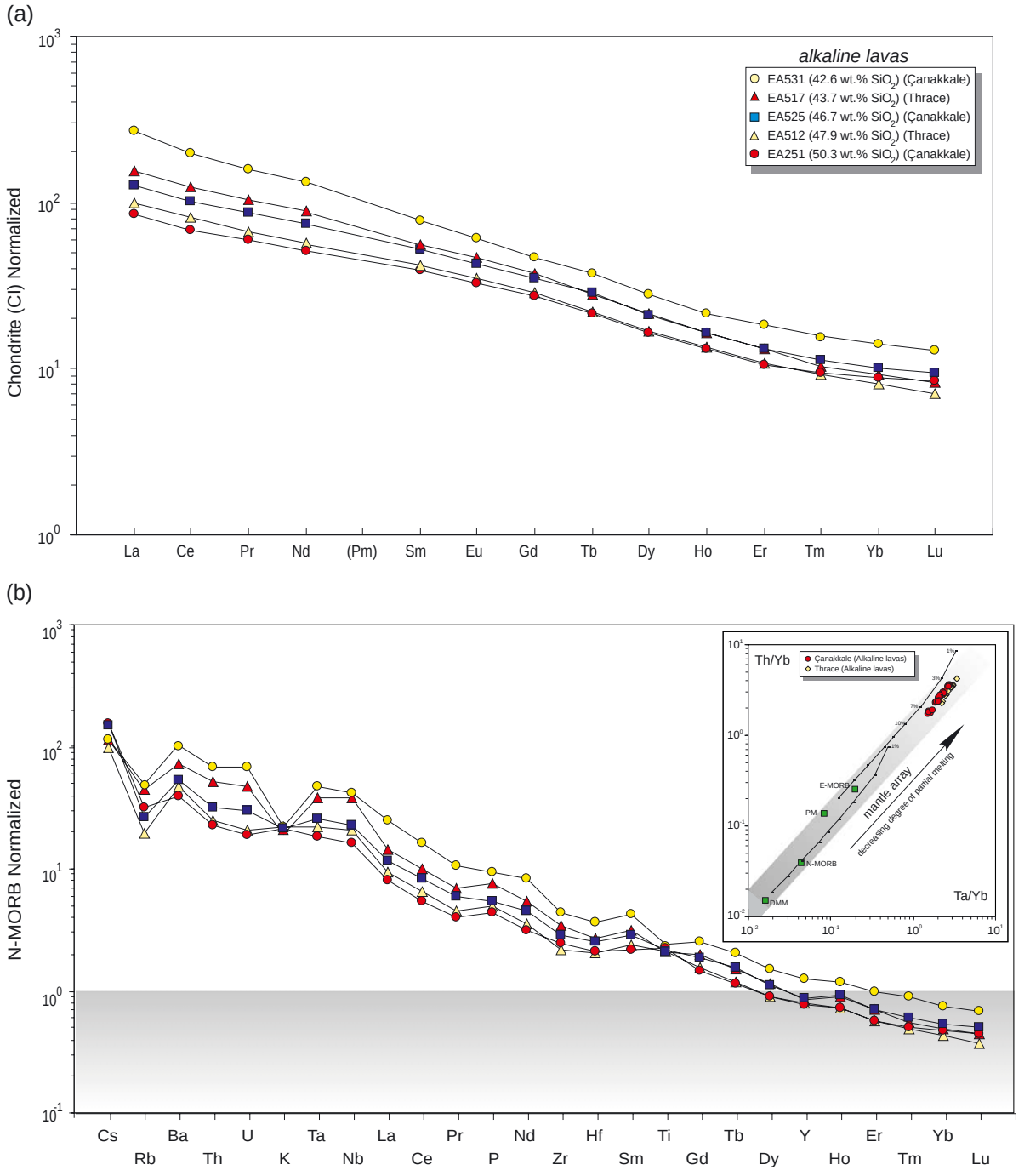

Fig. 3. (a) Chondrite-normalized REE element patterns for the alkaline volcanic rocks from NW Turkey. Chondrite normalizing values are from Boynton (1984). (b) N-MORB normalized multi-element patterns for the alkaline volcanic rocks from NW Turkey. N-MORB normalizing values are from Sun and McDonough (1989). The inset diagram shows the variation of Th/Yb vs. Ta/Yb for the volcanic rocks.

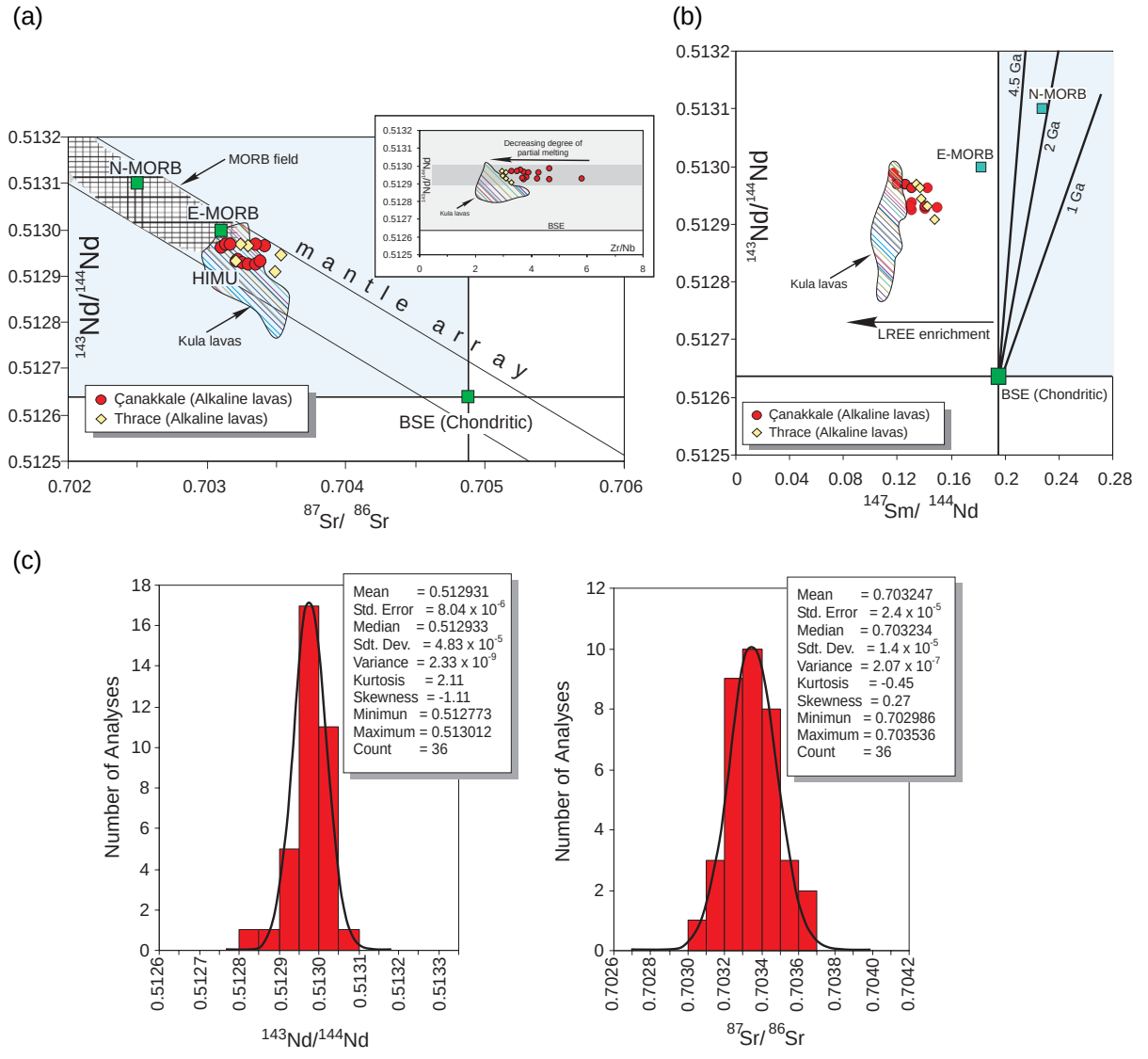

Fig. 4. (a) The Nd–Sr isotopic covariation shows that the Cenozoic alkaline volcanic rocks of NW Turkey plot in the mantle array extending from MORB-like compositions toward bulk Earth. MORB composition is from Zindler and Hart (1986); BSE (bulk silicate Earth) composition is from Hart et al. (1992). Also plotted for comparison are the samples from other Late Miocene to Quaternary mafic alkaline volcanic suites of western Turkey, including the Biga peninsula (Aldanmaz et al., 2000) and Kula (shown as shaded field; Alıcı et al., 2002; Aldanmaz, 2002 and references therein). The inset diagram shows the variation of $^{143}Nd/^{144}Nd$ ratios with changing Zr/Nb ratios throughout the sequences. (b) Plot of $^{143}Nd/^{144}Nd$ vs. $^{147}Sm/^{144}Nd$ showing the isotopically depleted and LREE-enriched nature of the volcanic rocks from NW Turkey. The heavy lines represent the mantle trends drawn for 4.5, 2.0 and 1.0 Ga from the hypothetical bulk silicate Earth which is often used as representing Primitive Mantle (BSE; Hart et al., 1992). (c) Sr and Nd isotopic distributions representing the entire volume of the Late Miocene to Quaternary mafic alkaline volcanic products from all over western Turkey, along with the statistical parameters derived from each distribution. Solid lines denote the fitted normal distributions.

incompatible element depletion, i.e. significant periods of evolution in LREE-depleted reservoirs (e.g. $[Nd/Sm]_{rock} < [Nd/Sm]_{BSE}$).

Fig. 4c shows the statistical distribution of $^{87}Sr/^{86}Sr$ and $^{143}Nd/^{144}Nd$ isotope ratios for the Late Miocene to Quaternary alkaline volcanic rocks from across western

Turkey, along with the statistical parameters derived from each distribution. The data mostly reveal normal distributions for both isotope ratios suggesting a restricted range of compositional variations in the source mantle. The skewness of the datasets, a measure of the asymmetry, is negligible for both Sr and Nd isotopic ratios, confirming the high degree of symmetry and central tendency for distribution of the isotopic ratios. Relatively low values for the excess kurtosis, the measure of a relative 'peakedness' or 'flatness' of a distribution, also reveal near-Gaussian distributions with high peakedness for both sets of isotopic ratios, leading to the suggestion that the source mantle from which the alkaline magmas were formed was not chemically heterogeneous and that the contribution from outliers (e.g. any possible sub-reservoir) was insignificant.

6. Petrogenetic implications

The alkaline rocks from NW Turkey offer an exceptional opportunity for using rock compositions to evaluate the mantle source characteristics and the processes of melt generation because the individual lava piles of cogenetic eruptions are spaced in time, providing a detailed geochemical dataset on temporally-controlled sequences of intra-plate magmas. It is evident from the restricted range of radiogenic isotopic ratios and near-constant concentration ratios of highly incompatible elements throughout the volcanic sequences that the lavas are cogenetic. Moreover, the magmas are relatively primitive, i.e. liquids generated by partial melting of a mantle source with little or no subsequent compositional modification, or their compositions can be confidently corrected for the effects of fractional crystallization. Specifically, well-developed correlations of highly incompatible elements enable us to use the rock compositions (or fractionation-corrected compositions) for modeling the source region characteristics and melting processes.

However, examining the type and extent of melting and the characteristics of the source mantle using the rock compositions strictly requires identification of shallow-level petrogenetic processes in low pressure magma storage areas (i.e., contamination and differentiation), as the geochemical signatures of primary melts are likely to have been modified by these processes. In the following sections we evaluate the possible effects of shallow-level processes in an attempt to remove any such effects from the primary melt compositions before considering any qualitative or quantitative modeling.

6.1. Crustal contamination

Several factors make crustal contamination an unlikely process for the eruptive sequences of mafic alkaline suite of NW Turkey. Specifically, no samples show negative Ta or Nb anomalies on MORB-normalized plots indicating an ascent of primary melt(s) with no significant crustal contamination. A Th/Yb vs. Ta/Yb plot (shown as inset in Fig. 3b) also indicates that the alkaline magmas have not been affected by any significant contamination for which a marked shift toward high Th/Yb ratios and displacement from the mantle array would be required. In general, the addition of crustal material to basaltic magmas or their source region is expected to produce a positive covariance of $^{87}Sr/^{86}Sr$ with parameters such as SiO_2, Rb/Sr, K_2O/P_2O_5 and Zr/Nb. This is, however, not observed throughout the lava sequences of NW Turkey, i.e. no correlation is observed between Zr/Nb ratios and isotopic ratios of the rocks (see the inset diagram in Fig. 4a) and $^{87}Sr/^{86}Sr$ change only slightly over a significant range of SiO_2 content from 42.6 to 50.3 wt.% (Table 2). The majority of the samples also have >6 wt.% MgO and Mg#>0.62, reflecting near primary melt composition for the alkaline suites. Furthermore, many of the lavas contain abundant ultramafic mantle xenoliths, indicating a rapid transit through the lithosphere and travel of magmas from their mantle sources to the surface without significant contamination.

6.2. Fractionation correction and primary melt composition

Basaltic magmas erupted within plate extensional settings are likely to have undergone variable degrees of low-pressure fractional crystallization that may affect the composition of the primary melts. In particular, the potential of olivine and clinopyroxene crystallization during mantle differentiation is a process that has some significance for the interpretation of intra-plate basalt compositions. Two criteria can be potentially used to identify 'primary' melts: (1) high concentrations of compatible trace elements (Ni, Cr, V, Sc) that are in equilibrium with mantle olivine (e.g.

Table 2
Nd–Sr isotope analyses for the representative samples from NW Turkey

Sample	Locality	Rock type	SiO_2 (wt.%)	Rb (ppm)	Sr (ppm)	$^{87}Sr/^{86}Sr$	Nd (ppm)	Sm (ppm)	$^{143}Nd/^{144}Nd$	ε_{Nd}
EA509	Thrace	Alk. Basalt	45.12	22.4	734.5	0.703241 ± 14	35.43	7.58	0.512970 ± 10	6.30
EA519	Thrace	Basanite	43.27	11.0	837.1	0.703536 ± 19	34.21	7.46	0.512945 ± 9	5.81
EA508	Thrace	Basanite	44.82	20.2	725.3	0.703295 ± 13	32.01	6.98	0.512964 ± 11	6.18
EA515	Thrace	Basanite	43.99	19.9	759.6	0.703209 ± 14	28.35	6.42	0.512931 ± 8	5.53
EA511	Thrace	Alk. Basalt	47.83	13.3	711.6	0.703492 ± 13	27.11	6.37	0.512908 ± 6	5.08
EA531	Çanakkale	Basanite	42.66	42.3	1056.2	0.703166 ± 14	59.93	11.35	0.512970 ± 8	6.32
EA527	Çanakkale	Basanite	44.69	13.5	882.7	0.703352 ± 14	42.31	8.44	0.512969 ± 6	6.30
EA526	Çanakkale	Alk. Basalt	45.79	18.4	1126.8	0.703409 ± 14	37.56	7.82	0.512964 ± 8	6.19
EA523	Çanakkale	Alk. Basalt	46.68	21.4	619.7	0.703376 ± 19	32.86	7.35	0.512931 ± 8	5.54

ε_{Nd} is reported relative to CHUR value of 0.512638. Errors quoted are the internal precision at 2SD.

Ni contents of 300–400 ppm); and (2) $Mg\#_{melt}$ in the range 0.68–0.76 (e.g. Frey et al., 1978) or Fe/Mg ratios within a range that is in exchange equilibrium with mantle olivine (e.g. Fo_{91}; Albarède, 1992). The basaltic primary melts should also be expected to precipitate olivine with $Fo_{88–91}$ (~90 Fo% where melting approaches the diopside-out curve).

The variation in major and trace elements in the alkaline rocks and in Fo contents of the olivine phenocrysts shows that none of the alkaline rocks from Çanakkale truly represent the primary melt, as their Ni and Cr contents are too low and Fe/Mg ratios are too high to be in equilibrium with mantle olivine, whereas most of the Thrace samples, with their Mg# of between 0.67 and 0.73, fulfill the criteria for being a representative of primary melt (Table 1; Fig. 5a). Existence of olivine phenocrysts in almost all alkaline samples from Çanakkale and some Thrace samples

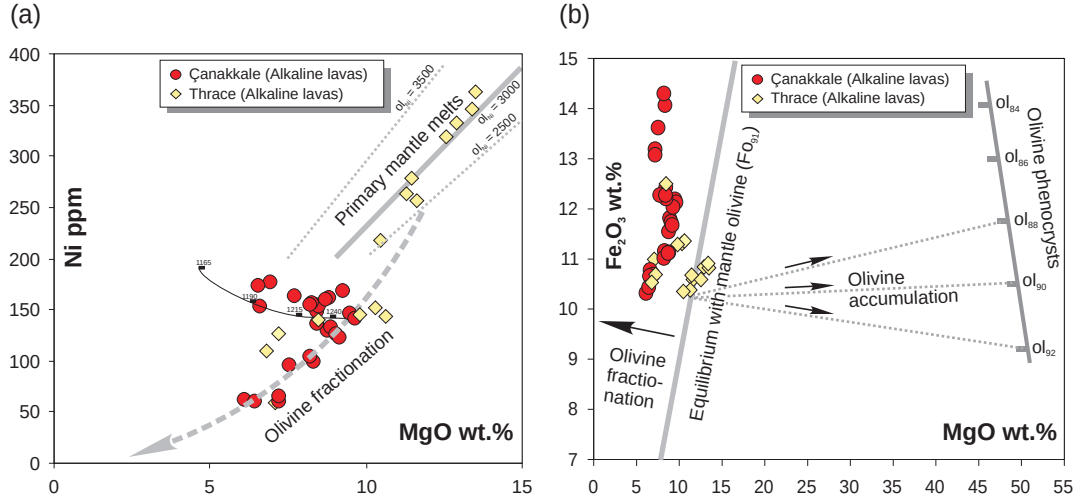

Fig. 5. (a) Ni vs. MgO relationships are compared with lines (or curves) for primary melts and the effects of olivine fractionation (Roeder and Emslie, 1970). Also plotted is a curve produced by high pressure (0.5 GPa), isobaric fractional crystallization of the most primitive sample from Çanakkale (EA531; Table 1) using the MELTS program. Thick marks on the curve correspond to decreasing temperature steps (liquidus; °C) as MgO decreases. Curves were calculated for an anhydrous system at the QFM buffer. Labels ol_{Ni}=2500–3500 indicate melts with equilibrium olivine containing 2500–3500 ppm Ni. (b) Plot of Fe_2O_3 vs. MgO showing the effects of olivine fractionation on primary melt compositions. Assuming a K_D $[(Fe/Mg)_{ol}/(Fe/Mg)_{melt}]$ of 0.3, a Fe_2O_3/MgO ratio of 0.9 can be inferred for the melt that is in equilibrium with the mantle olivine (Fo_{91}) and the Fe_2O_3 and MgO concentrations of the unfractionated (and noncumulated) liquid can be estimated. None of the samples from the alkaline volcanic suite of NW Turkey provide evidence for olivine accumulation, which would be expected to form linear trends of data points between the composition of the accumulated olivine (e.g. ol_{91}) and the line for melts in equilibrium with that olivine composition (e.g. Fo_{91}).

may further imply that their trace element abundances are likely to have been modified by varying degrees of low-pressure fractional crystallization, for which a correction is needed.

We therefore attempted here to invert the fractionation signature by adding liquidus phases, which are presumed to have fractionated during magma ascent, back into the magma to attain the primary melt composition(s). For the case of NW Turkish alkaline suite olivine fractionation appears to be the only significant compositional modification of the primary magma. We, therefore, used the olivine control lines (Fig. 5b) and the composition of the corresponding melts obtained by redissolving olivine until the melt is in equilibrium with olivine Fo_{91} (e.g. Albarède, 1992). Having estimated the amounts of the olivine that have been removed from the primary melt(s) to produce the observed melt (taken here as the measured compositions), trace element concentrations of each primary melt have been estimated from the observed melt using the Rayleigh fractionation law. The F value (mass fraction of liquid) for each sample has been calculated using Fe/Mg ratios of the samples and the olivine control line. The fractionation-corrected dataset for element concentrations used for the melt modeling is given in Table 1.

6.3. Trace element-based partial melting model: mantle compositions and extent of melting

The dynamic melting inversion (DMI) method proposed by Zou (1998) has been applied to the Late Miocene alkaline volcanic rocks of NW Turkey to estimate the source compositions and the degrees of partial melting independently. Several parameters should, however, be considered in producing the proposed model numerically; the densities of the melt (ρ_f) and the solid matrix (ρ_s) are assumed here to be 2800 and 3240 kg m^{-3}, respectively, and a value of 1% is selected as the critical melt fraction (or the porosity of the solid, in which some fraction of melt is retained in the form of a residual porosity; ϕ). For the modeling, aphyric or <10% phyric samples were selected to avoid any possible effect of mineral accumulation. The primary compositions used for the modeling, range from alkaline basalt to basanite and cover the whole compositional range of the mafic alkaline suite of NW Turkey.

For the calculations, Th was selected as a highly incompatible element ($D_{Th}<0.001$) to minimize the effect of the variations in the source mineralogy and the distribution coefficients. Lanthanum was selected as the second (less incompatible) component in order to achieve different enrichment ratios (Q_i) in magmas formed by different degrees of partial melting from a common source (Table 3). The bulk distribution coefficients for both the source mantle (D_i) and the extracted melt (P_i) were estimated using the mineral proportions and mineral/melt partition coefficients listed in Table 3. Using the enrichment ratios of (Q_{Th}) 2.69 and (Q_{La}) 2.90 between two end-member products of mantle melting (e.g. basanite; EA531 and an alkaline basalt; EA530), degrees of partial melting of 2.6% and 9.1% have been obtained by solving the equations proposed by Zou (1998).

Table 3
Estimation of partial melting degrees and mantle source composition for alkali basalts and basanites from NW Turkey

Element	D_i	P_i	Basanite (ppm)	Alkali Bas. (ppm)	Q_i	DMI		IBM		Co (ppm)
						$F1$ (%)	$F2$ (%)	$F1$ (%)	$F2$ (%)	
Th	0.00011	0.00021	5.71	2.12	2.70					
La	0.00559	0.03728	44.66	15.41	2.90	2.63	9.15	2.19	8.15	1.87
Ce	0.00916	0.06736	85.42	32.13	2.66	2.74	10.10	2.36	8.21	3.91
Nd	0.01942	0.05781	43.15	18.01	2.40	2.26	8.79	1.95	7.80	2.49
Ta	0.00722	0.0153	4.38	1.88	3.16	1.98	7.70	1.81	6.80	0.18
Nb	0.00782	0.01532	69.36	29.08	2.39	2.16	8.41	1.87	7.33	2.85
Average						2.35	8.83	2.04	7.66	

Partial melting degrees have been calculated using Concentration Ratio (CR) method with equations deduced from Zou (1998) and Maaløe (1994) for Dynamic Melting Inversion (DMI) and Incongruent Batch Melting (IBM) respectively. Source compositions were calculated using the mode and melt mode given in Kinzler (1997) and mineral melt partition coefficients given in McKenzie and O'Nions (1991, 1995) and Green (1994). D_i=bulk distribution coefficients for the solid source; P_i=bulk distribution coefficients for the extracted liquid; Q_i=enrichment concentration ratio; Co=source concentration; F=degree of partial melting.

For comparison, using the concentration ratio method for incongruent batch melting (IBM; Maaløe, 1994), degrees of partial melting have been calculated as 2.1% and 8.1% for the basanite and the alkaline basalt respectively. The difference between two methods is probably due to the (ϕ) value, which is not considered in the batch melt modeling. It should be noted that the estimated values of degree of melting are strongly dependent on the bulk distribution coefficients (D_i); uncertainties in the applied bulk distribution coefficients are likely to have caused significant variations in the estimated values of degree of melting. Thus, an average estimate based on several incompatible elements would be comparable and more useful. The calculations of the degree of melting have therefore been attempted with five different incompatible elements using both the DMI and IBM methods. The average estimates by the DMI method have been obtained as 2.3% ($\pm$0.4) and 8.8% ($\pm$1.3) for the basanite and the alkaline basalt end-member products respectively (Table 3).

The results are plotted on a chondrite-normalized REE diagram together with the whole compositional range of the alkaline rocks from NW Turkey and the DMM and PM values (Fig. 6). The estimated source concentrations range from 8.9 to 6.1 × CI for the LREEs, to 1.4 to 1.7 × CI for the HREEs when the source composition is taken as spinel-lherzolite. It should be noted that two different calculations based on two different X (the mass fraction of liquid extracted) values yield similar source concentrations for all the REEs. The calculations with the garnet-lherzolite composition, however, yield two different ranges of source concentrations for the HREE: 3.0 to 4.1 and 3.3 to 5.0 × CI respectively. An important point from these plots is that the estimated LREE concentrations of the source are invariably greater than those of the DMM (from 8.3 (La) to 3.6 (Nd) × DMM).

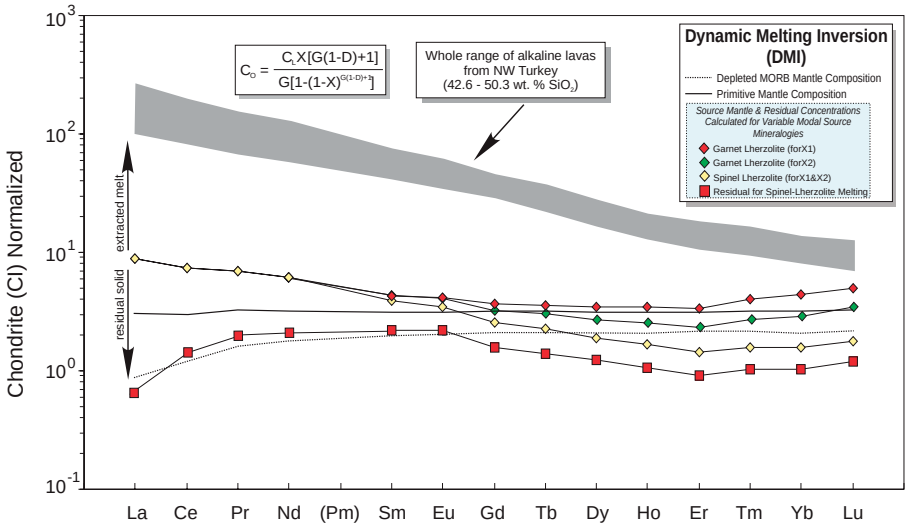

Fig. 6. Chondrite (CI) normalized REE patterns showing the model mantle source compositions (prior to melting) calculated by dynamic melting inversion (DMI) method (Zou, 1998) using the data from the mafic alkaline volcanic rocks from NW Turkey. The modeling uses the enrichment ratios of two different incompatible elements between two different but cogenetic primary magmas and the parameters described in Zou (1998). Source compositions were calculated for spinel-lherzolite (with mode and melt mode of $ol_{0.530}+opx_{0.270}+cpx_{0.170}+sp_{0.030}$ and $ol_{0.060}+opx_{0.280}+cpx_{0.670}+sp_{0.110}$ respectively; Kinzler, 1997) and for garnet-lherzolite (with mode and melt mode of $ol_{0.600}+opx_{0.200}+cpx_{0.100}+gt_{0.100}$ and $ol_{0.030}+opx_{0.160}+cpx_{0.880}+gt_{0.090}$ respectively; Walter, 1998). Normalizing values (CI) are from Boynton (1984); mineral/matrix partition coefficients are from the compilation of McKenzie and O'Nions (1991, 1995); PM and DMM compositions are from McDonough and Sun (1995). See Table 3 for the calculated source concentrations, the mass fraction of liquid extracted (X) and the bulk distribution coefficients used in the modeling. Also plotted for comparison is the model residual mantle composition calculated assuming an average of 6% melt segregation within the spinel stability field from a mantle source with incompatible trace element composition representative of the model mantle composition.

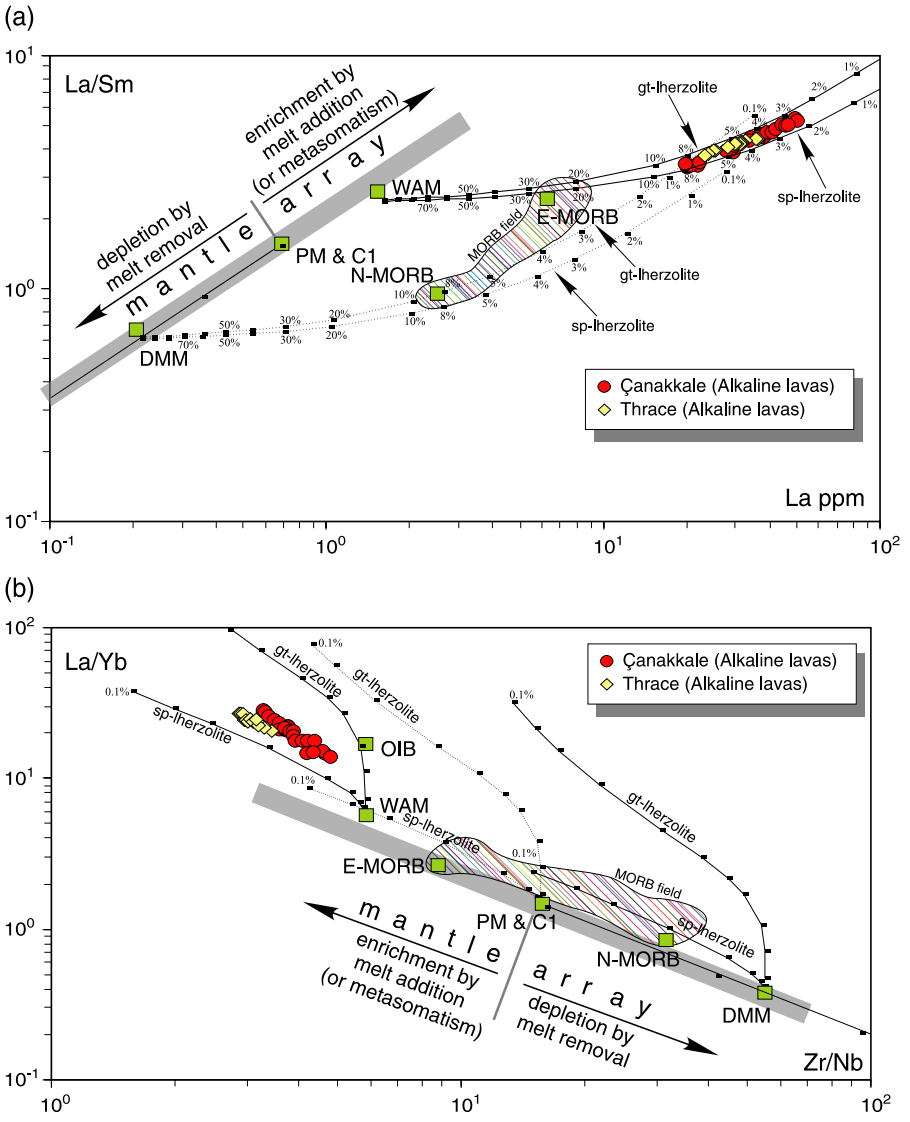

Fig. 7. (a)–(b) Plots of La/Yb vs. Zr/Nb and La vs. La/Sm showing melt curves (or lines) obtained using the non-modal batch melting. Melt curves are drawn for both spinel-lherzolite and for garnet-lherzolite (with mode and melt mode described in Fig. 6). Mineral/matrix partition coefficients and PM and DMM compositions are as described in Fig. 6; N-MORB and E-MORB compositions are from Sun and McDonough (1989); MORB data are from Niu et al. (2001). WAM represents the Western Anatolian Mantle (Aldanmaz et al., 2000) defined by dynamic melt inversion method of Zou (1998). The mantle array defined using melt-residual compositional trends from DMM and PM compositions. Mantle depletion and enrichment trends are defined by melt extraction from the mantle (towards the residues) and melt addition to the mantle (or influx of material from outside the mantle prior to solid-state mixing and homogenization) respectively. The melting trends from DMM and WAM compositions are shown by solid curves (or lines) while the dashed curves (or lines) represent the melting trends from PM. Thick marks on each curve (or line) correspond to degrees of partial melting.

The calculated parameters can also be used to reproduce the patterns displayed by the trace elements on any binary diagram such as La/Sm vs. La diagram (e.g. Aldanmaz et al., 2000) (Fig. 7a). The results show that partial melting trajectories drawn from the calculated model mantle source (shown as WAM) reproduce the alkaline rocks from NW Turkey by degrees of partial melting between ~2% and ~8%.

A more useful approach to melt modeling is the use of plots of highly incompatible to not so-highly incompatible element ratios (e.g. La/Yb vs. Zr/Nb). These plots are particularly useful, as their sensitivity to variations in the melting processes can distinguish (1) the effects of partial melting from those of fractional crystallization on a mantle-derived primary melt; (2) between melting of enriched and depleted (e.g. relative to PM) sources; and (3) between melting of garnet-and spinel-lherzolite sources (e.g. Aldanmaz, 2002).

Fig. 7b shows that the ratios of La/Yb and Zr/Nb vary widely in the NW Turkish alkaline samples and increasing Zr/Nb ratios are accompanied by decreasing La/Yb. The significantly large range of Zr/Nb ratios throughout the sequences cannot possibly be explained by fractional crystallization because the ratio of Zr/Nb is not affected significantly by fractionation of mantle phases. Given that the rocks are cogenetic, possible long-lived mantle heterogeneity also cannot explain the observed Zr/Nb ratios. Variable degree of partial melting is thus clearly the simplest, and perhaps the only, explanation to account for the variation in highly incompatible to not so-highly incompatible element ratios that are not associated with isotopic variability, as samples representing smaller degree of partial melting are expected to show higher incompatible element concentrations and highly incompatible to not so-highly incompatible element ratios (e.g. Nb/Zr and La/Yb).

The modeling in Fig. 7ab also shows that the NW Turkish alkaline volcanic rocks have La/Yb ratios greater and Zr/Nb ratios smaller than those could be generated by a single-stage melting of DMM (or even PM), even when the degree of partial melting is unrealistically small (0.1%). Thus, it can be argued that the one-stage melting of DMM or PM cannot produce magma with incompatible element ratios similar to those of the alkaline rocks from NW Turkey. Clearly, an enrichment event (either source- or process-related) is required to produce the composition of the alkaline rocks.

7. Inferences about the nature of mantle source

The quantitative modeling of melt compositions shows that, using conventional melting equations, it is possible to reproduce trace element compositions of the alkaline magmas of NW Turkey by 2% to 8% melting of a peridotite source, with minor and trace element abundances slightly different from those of Primitive Mantle. The average source inferred for the alkaline rocks, has La concentrations and La/Sm (and Nb/Zr) ratios greater than that of Primitive Mantle. The relative source concentrations, calculated using an inverse numerical method presented above, also show that the modelled mantle source for the alkaline magmas was enriched in all highly (and moderately) incompatible elements relative to the hypothetical DMM and PM values. The degree of enrichment, as observed in many OIB settings, increases systematically in order of increasing incompatibility, resulting in enrichments of light over heavy REE and highly-incompatible over less-incompatible elements compared to the DMM and/or PM compositions. The isotopic results, however, reveal an isotopically depleted (e.g. relative to BSE) mantle source for the alkaline lavas of NW Turkey, emphasizing that the postulated enrichment of the lavas is a recent (possibly a process-related) event and not a long-term source characteristic.

Recent enrichment, which refers to enrichment in more incompatible relative to less incompatible elements during or after melt segregation from the mantle, is essentially observed in the vast majority of OIB settings and could simply be attributed to two potential processes: (1) mixing of melts from two or more chemically distinct end-members; and (2) melt (or fluid)–rock reactions associated with extensive porous flow.

7.1. Multi-component mantle interaction and potential end-members

Systematically changing proportions of mixing between melts produced by variable degrees of partial melting of at least two compositionally distinct

sources in the mantle is generally invoked to explain both isotopically depleted (e.g. relative to BSE), but LREE-enriched nature of many OIB-type alkaline suites and the quasi-linear patterns between highly incompatible elements observed in OIB-type rocks. Several recent studies regarding trace element and isotope compositional variations on relatively short time scales and length scales have suggested binary mixing as a dominant source of chemical variation in alkali primary suites (e.g. Class and Goldstein, 1997; Kamber and Collerson, 2000). In this context, the most likely hypothetical end-member reservoirs are presumed to be located in a number of rheologically distinct (and accessible?) parts of the mantle, including plume components (e.g. originating below the convectively stirred upper mantle), and convective and conductive mantle sources. The processes of mixing melts from two or more compositionally distinct end-member sources generally involve either the addition of incompatible element-enriched plume-derived melts or fluids to a depleted (e.g. DMM-like) mantle source prior to melt generation or, alternatively, addition of incompatible element-depleted mantle-derived melts to an enriched conductive mantle source (e.g. Lassiter et al., 2000). Thus, several recent studies regarding OIB-type magma genesis assume that the resulting lavas in these environments are pooled and mixed melts and that the magma generation is inevitably related to either a plume origin or involvement of melts from conductive mantle, or both (e.g. Lundstrom et al., 2003).

The plume hypothesis, i.e. in the sense of deep-seated thermal anomalies, assumes (perhaps unrealistically) the convecting upper mantle to be cold, dry and significantly subsolidus, and generally attributes magma generation to temperatures of approximately 250–300 °C above the ambient temperature to achieve sufficient melt for intra-plate basalt provinces (despite the volatile-rich nature of most intra-plate sources). There are, however, numerous problems reconciling the observations with a plume model in NW Turkey. Extensional stress associated with the lithospheric uplift, for instance, should be the maximum above a plume apex, which in turn would be expected to create an uplift and doming structure as a surface manifestation of such thermal anomaly. This is, however, not observed in the alkaline field of NW Turkey, nor is there any evidence for locally elevated temperatures. In fact, the evidence from surface heat flow measurements and mineral equilibrium constraints (Pfister et al., 1998; Aldanmaz et al., 2005) suggest that the thermal gradient in NW Turkey is not anomalously high. In addition, pinpoint thermal and stress perturbation expected by adiabatically upwelling mantle plume is inconsistent with linearly distributed patterns of the volcanic centers as well as planar geometry of normal or even strike-slip faulting of NW Turkey, where the small volume and discontinuous (or episodic) generation of alkaline magma is related mostly to strike-slip (or transcurrent) deformation.

Furthermore, for the case of NW Turkish alkaline volcanic suite, there is no clear indication of a change in depth, i.e. from garnet-to spinel-facies mantle, as might be expected for an actively upwelling mantle plume, nor is there any dramatic change in the degree of partial melting, as might be expected for a dynamic mantle plume, potentially increasing to very large degrees of partial melting. The alkaline lavas from NW Turkey display a trend of significant enrichments in incompatible trace elements and a gradual decrease in silica content with decreasing eruption age. Such a compositional trend can be interpreted in terms of progressively increasing depth of melting coupled with decreasing degree of melting of a compositionally uniform source, which is inconsistent with a possible plume hypothesis.

Involvement of melts from conductive mantle in the genesis of OIB-type magmas is usually considered as a common process owing partly to the ability of the conductive mantle to remain isolated from mantle convection for a geologically reasonable period of time to create anomalous isotopic signatures of most OIB magmas compared to MORB. Existence of residual hydrous minerals such as amphibole or phlogopite (evident from the classic negative K and Rb anomalies in most OIBs) is another reason why many researchers believe that involvement of conductive mantle-derived melt in the OIB genesis is inevitable (e.g. Class and Godstein, 1997). Melt derivation from conductive mantle in the genesis of the alkaline magmas of NW Turkey is unlikely however; as noted by Aldanmaz et al. (2000), the mantle lithosphere beneath western Turkey is subduction-modified, and any model involving melts from such a source would produce magmas with significant arc signatures.

Melt contribution from the conductive mantle is also inconsistent with the temporal compositional trends observed in the alkaline basaltic sequences of NW Turkey. During melt migration and ascent, hydrous phases and other fusible components in lithospheric channels would be expected to have been progressively exhausted as melting proceeds. This depletion would generate initial batches of melt having the strongest signature of residual hydrous phases and a temporal compositional trend reflecting the exhaustive capacity of such phases in sequentially erupted batches of melt. The resultant magmas would therefore be expected to show the strongest negative K and Rb anomalies in the leading batch of melt with a time-dependent decrease, which is opposite the trend we observe throughout the lava sequences of NW Turkey.

Isotopic constraints provide another strong line of evidence against melt generation by mixing melts from multiple sources. The alkaline rocks that formed over a significant period of time have near-constant Sr and Nd isotopic ratios, and incompatible element concentration ratios for the entire suite, indicating that melt generation is likely to have taken place under conditions of significant chemical homogeneity, probably within a single mantle domain. Therefore, any model proposed to account for the chemical composition of the alkaline magmas from NW Turkey should be able to describe melt generation within a well-homogenized system with no contribution from a source selectively enriched in mobile incompatible elements. The best site for this apparent chemical homogenization, which might possibly require premelting, solid-state mixing of discrete mantle lithologies (created by plate recycling processes) would be a sub-lithospheric convective (i.e. well-stirred, homogeneous) system (e.g. Hofmann, 1997; van Keken et al., 2002; Kellogg et al., 2002).

If interpreted in a regional context, the NW Turkish alkaline lavas exhibit strong similarities in terms of trace element and isotopic compositions with coeval widespread alkaline magmatism formed in very similar geological setting throughout western, central and eastern Europe (the so-called "European Volcanic Province" = EVP; Wilson et al., 1995). In particular, geochemical characteristics of the NW Turkish alkaline rocks are almost identical to the HIMU end-member of the EVP volcanism, which is referred in the literature as to the Lower-Velocity-Component (Hoernle et al., 1995) or the European Asthenospheric Reservoir (Wilson et al., 1995). This component seems to be a hallmark of mid-plate basalts that characterize a tectonic regime dominated by plate convergence and collision followed by later-stage extension and is likely to represent compositional, rather than thermal, anomaly zones within the shallow convective mantle (i.e. partially molten, shallow fertility anomaly zones).

7.2. Chemical exchange reactions during melting and melt transport

The chemical reaction between segregated melt and the surrounding solid residue during melt transport is considered as an important mechanism to modify the composition and volume of melt (e.g. Hauri, 1997). This type of reaction may particularly be important in cases when local equilibrium between migrating melt and solid mantle is achieved. In other words, a chemical reaction between melt and solid mantle is possible only if the time to reach equilibrium between melt and solid is sufficiently shorter than the residence time of melt in the mantle. Experimental studies have shown that equilibrium between melt and the surface of solid grains is attained within relatively short periods (i.e., 24 h) at temperatures higher than 1200 °C, and even the surface equilibration can change the melt compositions significantly (e.g., Hirose and Kushiro, 1998; Kogiso et al., 1998). In this context, some argue that chromatographic migration of highly incompatible element depleted melts through residual mantle peridotites may be an efficient mechanism to produce highly incompatible element enriched melts (e.g. Takazawa et al., 1992).

In this type of metasomatic scheme, elements move through porous peridotites with diffusive velocity inversely proportional to their solid/melt partition coefficients. Under certain conditions, infiltrating melts can be equilibrated with incompatible elements in mantle peridotites during melt migration and ascent, preferentially leaching incompatible elements from the mantle peridotites. This type of melt-rock interaction produces magma batches with high ratios of highly incompatible to less incompatible elements relative to the original parental melt composition.

Trace element characteristics of the alkaline lavas from NW Turkey strongly suggest that melt/solid interaction may have played a significant role in generating the compositional variations of the alkaline melts. The process of melt metasomatism in the source region of the alkaline magma(s) from NW Turkey can be considered as an autometasomatic event, a process related to the reaction between solid source and LREE-enriched reactive agent which was presumably derived from the same source as the alkaline magma. This agent (or small melt fractions) is likely to be hydrous in character, judging from significant Rb, K and Ti depletion relative to neighboring incompatible elements on multi-element patterns (e.g. Fig. 3a). Such depletions, observed even in the freshest samples, do not seem to be associated with a similar behavior of other highly mobile elements (e.g. Ba in particular) implying that atmospheric processes are unlikely to be the main cause of these negative anomalies. Likewise, the lack of correlation between behavior of K and those of other fluid-soluble large cations preclude the possibility of explaining these negative anomalies solely by the presence of dehydrated oceanic crust in the source of the alkaline melts.

Partition coefficients for highly incompatible trace elements are well established for common mantle minerals and do not allow significant fractionation between adjacent elements on an N-MORB normalized diagram such as illustrated in Fig. 3b. Given the similar bulk partition coefficients for these highly incompatible elements in either spinel-or garnet-lherzolite, K will not be fractionated from either Th or Nb during partial melting and, on a plot of K/K* vs. La, melting trajectories drawn for conditions of dry melting will be horizontal (Fig. 8a). Therefore, the negative correlations shown by the alkaline volcanic rocks from NW Turkey in Fig. 8a can be explained only if K behaved as a considerably more compatible element than either Th or Nb. To effect the necessary fractionation of K from Th and Nb requires either crystallization of K-bearing phase or buffering against a K-bearing phase during melting in the mantle. The first option seems unlikely for the case of NW Turkish alkaline suite, as there is no evidence of amphibole or phlogopite having crystallized from any of these alkaline magmas. The most likely explanation for such a systematic depletion is thus the presence of a residual K (Rb, and Ti) retaining phase in the source region (e.g. phlogopite or amphibole) as the melting trajectories drawn using a compilation of partition coefficients between phlogopite-and amphibole-silicate melts show that residues of either mineral in the source mantle would create roughly similar-sized negative anomalies for these elements (Fig. 8ab).

However, one might question the possibility of long-term stability of the inferred hydrous minerals in a steady-state convecting system, as these phases are not particularly common primary mantle minerals. Although the maximum temperature of stability for amphibole is dependent on the source composition, especially total alkali content (e.g., Niida and Green, 1999), no experimental studies have demonstrated amphibole stability at mantle potential temperatures greater than 1300 °C even in alkali-rich peridotites. Likewise, primary phlogopite is unlikely to be stable at depths shallower than ~160 km (Sato et al., 1997) unless the mantle potential temperature is significantly low. Presence of the inferred hydrous phases in the original, pre-melting, solid mantle also is inconsistent with the temporal compositional trend of the lavas; irrespective of the nature of mantle origin, either convective or conductive, the time-integrated fusion of these phases would be expected to result in a decrease in the hydrous character of the magmas as melting proceeds. The inferred hydrous minerals are notably not primary phases in the source mantle, but might be the short-lived products of metasomatic reaction which presumably took place during melting and melt migration through intergranular channels.

A complementary evidence for the process of source metasomatism by migrating melt may be that the depletion in Rb, K and Ti correlates with both time and the degree of partial melting (but not with the isotopic ratios) and, as shown in the K/K* vs. La plots (Fig. 8a), the degree of depletion increases gradually in time toward the most primitive sample (the product of the smallest degree of melting with the greatest liquidus temperature) implying a time-integrated increase in the extent of source metasomatism. Such correlation is also consistent with the recent quantitative model of Asimow and Langmuir (2003) and suggests that in upper mantle melting regimes with increasing the water content of the source, the mean extent of melting

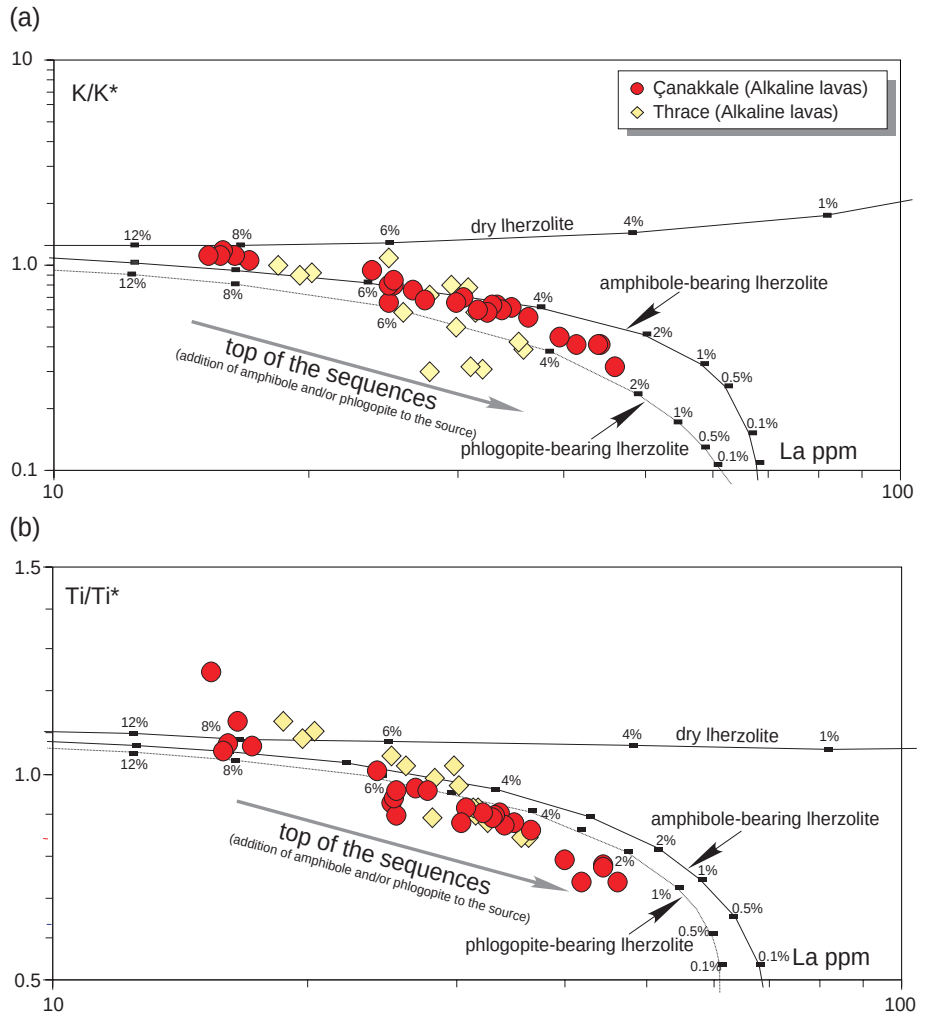

Fig. 8. (a)–(b) Covariation of K/K* and Ti/Ti* (taken as K and Ti negative anomalies) with changing La contents of the rocks. K* and Ti* have been taken as extrapolated K and Ti calculated using normalized concentrations of Th, K, Nb, and Sm, Ti, Gd respectively. Melt trajectories are drawn for (1) dry lherzolite ($ol_{0.530}+opx_{0.270}+cpx_{0.170}+sp_{0.030}$; Kinzler, 1997); (2) amphibole-bearing lherzolite ($ol_{0.558}+opx_{0.201}+cpx_{0.076}+sp_{0.115}+amp_{0.050}$); and (3) phlogopite-bearing lherzolite ($ol_{0.558}+opx_{0.201}+cpx_{0.076}+sp_{0.115}+phl_{0.050}$) sources using the non-modal batch partial melting of Shaw (1970). Melting of amphibole- and phlogopite-bearing lherzolites is assumed to initiate in dry condition but continues with addition of the inferred hydrous phases by up to 5%. Partition coefficients used are from the compilation of McKenzie and O'Nions (1991, 1995), Green (1994) and LaTourette et al. (1995).

decreases and incompatible element enrichments increase substantially.

8. Nature of the mantle melting

Fig. 9a shows model partial melting trends for typical mantle conditions together with the plots of the alkaline basaltic compositions from NW Turkey. The model liquid compositions produced using continuous fractional or dynamic melting models from a single source of either garnet-or spinel-peridotite compositions with any reasonable range of modes, initial trace element composition, and bulk distribution coefficients are expected to form curvilinear trends on a plot of Nd against La (La and Nd represent concen-

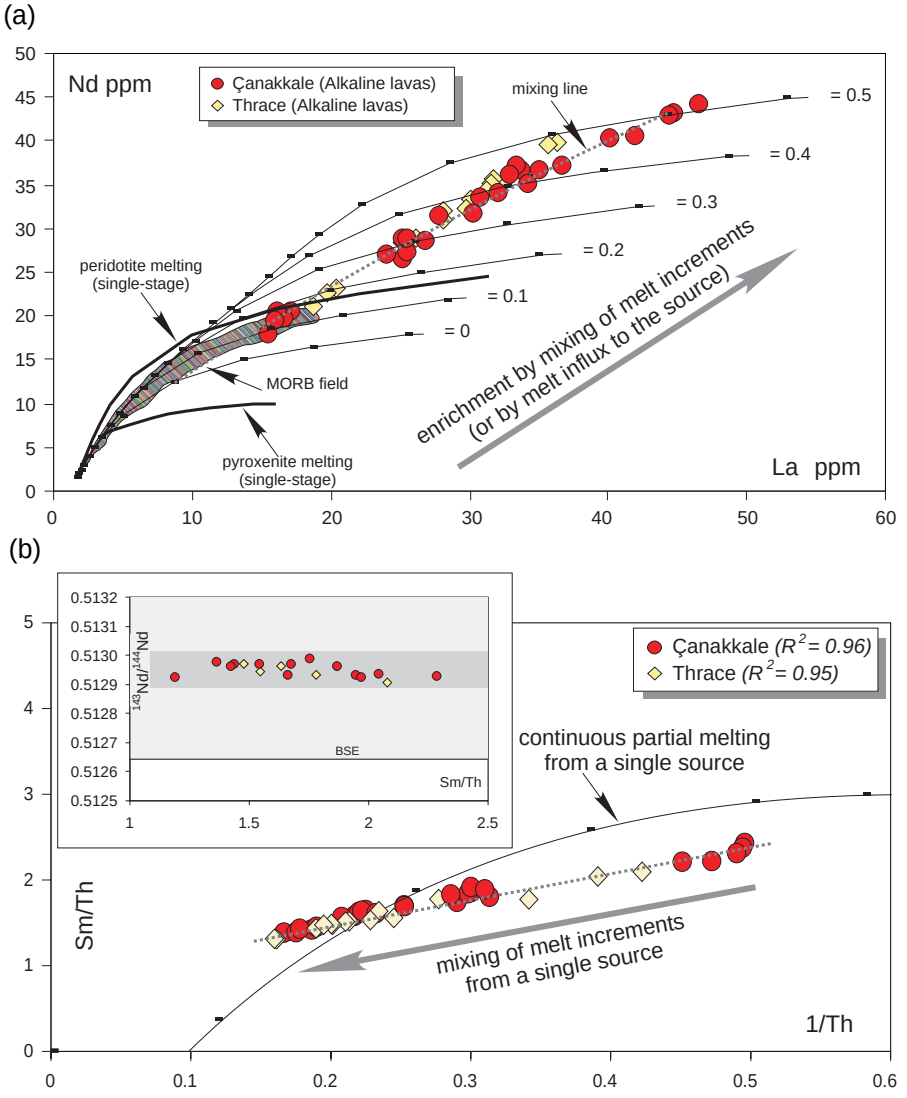

Fig. 9. (a)–(b) Plots of highly- vs. moderately incompatible elements and element ratios (La vs. Nd and Sm/Th vs. 1/Th) for the fractionation-corrected (primary) melt compositions calculated using the data from the alkaline lava sequences of NW Turkey. Also plotted the model partial melting curves (or lines) for both pyroxenite and peridotite (the solid curved lines) obtained using the non-modal batch melting equations of Shaw (1970). Source compositions and mode and melt mode for peridotite are as described in Fig. 6. Pyroxenite mode is assumed to be $cpx_{0.750}+gt_{0.250}$ with composition of average mantle pyroxenite from the dataset of Hirschman and Stolper (1996). Continuous partial melting of any single source predicts curved trends for moderately vs. highly incompatible elements. In contrast, highly and moderately incompatible trace elements from the lava sequences of NW Turkey generally exhibit quasi-linear trends suggesting a mixing between increments of melt derived from the same source but probably at different depths. The curves represent melting trajectories derived from a sequence of melting processes using the open system mass conservation equation of Ozawa (2001). Melting is assumed to initiate from a composition similar to that of DMM, but in each step of melting episode the source is modified by influx of melt from previous melting step until the composition of the source mantle modeled for western Turkey was attained. The strait dashed line represents a mixing line between small-degree melt increments produced during the sequential melting episodes. The numbers correspond to the rate of melt influx to the solid source following each step of melting. MORB data are from Niu et al. (2001).

trations of highly incompatible and less incompatible elements respectively) especially at less than 10% partial melting. The rate of depletion of the highly incompatible element with progressive melting is significantly higher than that of less incompatible element. Trace element variations in the alkaline lavas, however, are characterized by quasi-linear patterns with significantly high correlation coefficient values rather than curvilinear trends (Fig. 9a). In order for single-source partial melting to be a viable mechanism to produce the alkaline magmas by single-stage instantaneous melting and melt extraction, the source mantle would have to be extremely enriched in incompatible elements (e.g. $>10\times$CI for the LREE), which is not consistent with the results of inverse modeling presented above. Magma generation by continuous melting from a single mantle source (e.g. a system from which melts are continuously removed and chemically isolated from residues with a probable small proportion of residual porosity left behind) seems therefore difficult to reconcile with incompatible trace element relationships of the eruptive sequences of the alkaline lavas of NW Turkey.

Quasi-linear variations between incompatible trace elements are very common in intra-plate alkaline basaltic suites, and are, in most cases, attributed to the mixing of melts from heterogeneous lithological domains within the mantle. In this context, many suggest a binary mixing of melts to account for linear incompatible trace element trends as well as incompatible element-enriched patterns observed in many intra-plate alkaline suites. The origins of the suggested end-member components vary widely, but are generally restricted to erupted melt compositions with contrasting incompatible trace element concentrations. A widely accepted view is that the mixing of melts from depleted lherzolite and chemically enriched mafic veins (e.g. garnet pyroxenites) embedded in a peridotite matrix can account for both the quasi-linear patterns of incompatible elements and incompatible element enrichment observed in OIB-type magmas (e.g, Lassiter et al., 2000). This view is partly based on the common assumption that the preferential melting of lower-solidus-temperature pyroxenite veins will produce melts significantly enriched in incompatible elements relative to peridotite-derived melts and that variable proportions of mixing between pyroxenite- and peridotite-derived melts can account for the large range of isotopic variations observed throughout most OIB settings (e.g. Phipps Morgan, 1999; Kogiso et al., 2004). However, modeling in Fig. 9a shows that the first prediction is not necessarily true, as for a given source composition and with a set of chosen parameters, sources with higher abundances of clinopyroxene (e.g. pyroxenite) produce low degree melts with significantly lower concentrations of incompatible elements than either peridotite-derived melts or that would account for the compositions of the alkaline lavas of NW Turkey. Clinopyroxene (and garnet) have relatively high solid/melt partition coefficient for highly and moderately incompatible elements compared to other common mantle minerals. Mixing between pyroxenite- and peridotite-derived melts to create the quasi-linear variations of incompatible elements observed in the alkaline lavas of NW Turkey would therefore still require the peridotite end-member to be extremely enriched in incompatible elements, in which case there would be no need for contribution from a pyroxenite source.

Almost complete absence of silica-saturated compositions (e.g. tholeiites) throughout the lava sequences may further argue against significant role of pyroxenite melting in the genesis of alkaline lavas from NW Turkey, because melts of pyroxenite would be expected to be dominated by incongruent melting of orthopyroxene and hence have relatively high silica contents. In addition, although the wide variety of radiogenic isotope ratios in OIB global distribution is, in most cases, attributed to contribution from diverse components and large-scale mantle heterogeneities, eruption sequences of the alkaline lavas from NW Turkey show significantly restricted range of radiogenic isotope ratios, which is the opposite of what would be required in support of an origin involving mixing melts from lithologically (and isotopically) heterogeneous sources. Furthermore, note that the composition of resulting magmas that have been produced by processes of mixing of variable batches of magma from two (or more) lithologically distinct sources will deviate from any quasi-linear or curvilinear array on a plot of highly incompatible/moderately incompatible element against highly incompatible element (e.g. Th/Sm vs. Th), as mixing between compositionally contrasting sources will cause scatter.

A proposal that the alkaline magmas are the products of dynamic melting processes involving mixing

between the increments of melt derived from the same source but probably at different depths (e.g. Langmuir et al., 1992) would provide a much more satisfactory explanation. The extraction of melts that integrate over different pressure intervals within the melting regime and mixing between end-member components with similar incompatible element concentration ratios (but with different absolute concentrations of incompatible elements) will produce linear correlations between incompatible trace elements (with different incompatibilities) without causing any scatter (Fig. 9a).

A more compelling line of evidence indicating that the within-suite variations are due to mixing of melt increments from a single source is demonstrated using the plot of Sm/Th vs. 1/Th (Fig. 9b). The straight line array on the diagram is not consistent with continuous (e.g. fractional) melting using the commonly accepted mineral/melt partition coefficients, nor can it be explained by mixing of melts from discrete mantle components. Instead the linear array strongly suggests that the within suite variations can be interpreted in terms of mixing of melts produced by variable degrees of melting from a single mantle domain that was chemically homogenized before the inception of melting event. It is, thus, more appropriate to envisage a mixing between individual melt increments that are produced by variable degrees of partial melting from a single and isotopically homogeneous mantle source, perhaps under conditions of which significant equilibration was established between melts and the residual solid. The process envisaged can be presented as sequences of incremental (stepped) episodes of melting.

9. Concluding remarks

The Late Miocene mafic alkaline suite of NW Turkey comprises a series of scattered outcrops of lava flows formed along the localized extensional zones. The alkaline rocks mostly classified as alkaline basalts, basanites and trachybasalt with their low silica contents ranging between 43 and 50 wt.%. In general, they show OIB-like trace element patterns characterized by overall enrichment in LILE, HFSE, LREE and MREE, and a slight depletion in HREE relative to the N-type MORB composition.

The alkaline magmas have been shown to have originated from variable degrees (~2% to ~8%) of partial melting of an isotopically homogeneous, volatile-bearing, single mantle domain which is enriched in incompatible elements relative to DMM and PM compositions. Significant depletion in isotopic ratios of the lavas (e.g. relative to BSE) indicates that the apparent disagreement between isotopic and trace element signatures can most likely be explained by a relatively young (and process-related) event that enriched either the source mantle or the melts produced or both during the various stages of melting episodes.

There is no indication of a change in depth, i.e. from garnet-to spinel-facies mantle, as might be expected for an actively upwelling mantle as a plume, nor is there any dramatic change in the degree of partial melting, potentially increasing to very large degrees of partial melting. Geochemical evidence indicates that, on average, the alkaline lavas were generated by small degrees of partial melting probably within the spinel stability field and temporal compositional trend of the lavas indicate a progressively increasing depth of melting coupled with decreasing degree of melting of a compositionally uniform source. This, along with the other geochemical signatures of the lavas (e.g. constraints against melt contribution from the conductive mantle), suggests that melting is likely to have occurred within the convecting system.

The alkaline lavas from all over NW Turkey have near-constant Sr and Nd isotope ratios for the entire suite and systematic change in incompatible trace element compositions (and ratios) of the lavas is not reflected in the isotopic ratios, leading to the suggestion that the temporal compositional trends are not caused by source variations. Instead, the observed chemical trends can be interpreted as being a function of pressure (P) and degree of melting (F), implying that parts of the isotopically homogeneous (and a single) source are sampled systematically as a function of pressure and degree of melting. Such an argument can therefore preclude the possibility of variable proportions of mixing between melts from discrete mantle components in the genesis of the alkaline magmas.

Systematic variations in melt chemistry indicate that the alkaline magma generation is consistent with both the extraction of melts that integrate over different pressure intervals within the melting regime and mixing between end-member components with similar isotopic and incompatible element ratios but significantly different absolute concentrations of in-

compatible elements. Trace element and isotopic characteristics show that the simplest explanation is that the alkaline lavas are the products of integrated melting episodes that produce small volume melts. Interaction of such melts with the residual mantle metasomatises (and enriches) the local mantle regions and causes precipitation of hydrous mineral phases that were not initially present in the solid mantle (e.g. amphibole or phlogopite). Systematic mixing between melts produced in various stages of melting episodes can also account for the trace element and isotopic variations throughout the lava sequences.

Acknowledgements

Funding for trace element analyses was partly provided by the Engineering Faculty Society of Kocaeli University. Kocaeli University funding through a research project grant (2001/30) enabled us to carry out a part of the fieldwork. We appreciate the help by R.G. Hardy, C.J. Ottley (Durham University) and C. Bosq (University of Clermond-Ferrand) on XRF, ICP–MS and isotope analyses, respectively. We thank Cemal M. Göncüoglu for allowing us to use his sample preparation laboratories at the Middle East Technical University. Detailed and constructive reviews and helpful suggestions by S. Foley and an anonymous referee improved the manuscript significantly. The whole work was financially supported by TUBITAK grant YDABAG-102Y069.

References

Albarède, F., 1992. How deep do common basalts form and differentiate? Journal of Geophysical Research 97, 10997–11009.

Aldanmaz, E., 2002. Mantle source characteristics of alkali basalts and basanites in an extensional intracontinental plate setting, western Anatolia, Turkey: implication for multi-stage melting. International Geology Review 44, 440–457.

Aldanmaz, E., Pearce, J.A., Thirlwall, M.F., Mitchell, J.G., 2000. Petrogenetic evolution of Late Cenozoic, post-collision volcanism in western Anatolia, Turkey. Journal of Volcanology and Geothermal Research 102, 67–95.

Aldanmaz, E., Gourgaud, A., Kaymakçi, N., 2005. Constraints on the composition and thermal structure of the upper mantle beneath NW Turkey: evidence from mantle xenoliths and alkali primary melts. Journal of Geodynamics 39, 277–316.

Alıcı, P., Temel, A., Gourgaud, A., 2002. Pb–Nd–Sr isotope and trace element geochemistry of Quaternary extension related alkaline volcanism: a case study of Kula region (western Anatolia, Turkey). Journal of Volcanology and Geothermal Research 115, 487–510.

Asimow, P.D., Langmuir, C.H., 2003. The importance of water to oceanic mantle melting regimes. Nature 421, 815–820.

Boynton, W.V., 1984. Geochemistry of the rare earth elements: meteorite studies. In: Henderson, P. (Ed.), Rare Earth Element Geochemistry. Elsevier, pp. 63–114.

Class, C., Goldstein, S.L., 1997. Plume–lithosphere interactions in the ocean basins: constraints from the source mineralogy. Earth and Planetary Science Letters 150, 245–260.

Frey, F.A., Green, D.H., Roy, S.D., 1978. Integrated models of basalt petrogenesis: a study of quartz tholeiites to olivine melilitites from SE Australia utilizing geochemical and experimental petrological data. Journal of Petrology 19, 463–513.

Green, T.H., 1994. Experimental studies of trace-element partitioning applicable to igneous petrogenesis — sedona 16 years later. Chemical Geology 117, 1–36.

Hart, S., Hauri, E.H., Oschmann, L.A., Whitehead, J.A., 1992. Mantle plumes and entrainment. Science 256, 517–520.

Hauri, E.H., 1997. Melt migration and mantle chromatography: 1. Simplified theory and conditions for chemical and isotopic decoupling. Earth and Planetary Science Letters 153, 1–19.

Hirose, K., Kushiro, I., 1998. The effect of melt segregation on polybaric mantle melting: estimation from the incremental melting experiments. Physics of the Earth and Planetary Interiors 107, 111–118.

Hirschman, M.M., Stolper, E.M., 1996. A possible role for garnet pyroxenite in the origin of 'garnet signature' in MORB. Contributions to Mineralogy and Petrology 124, 185–208.

Hoernle, K., Zhang, Y.S., Graham, D., 1995. Seismic and geochemical evidence for large-scale mantle upwelling beneath the eastern Atlantic and western and central Europe. Nature 374, 34–39.

Hofmann, A.W., 1997. Mantle geochemistry: the message from oceanic volcanism. Nature 385, 219–229.

Kamber, B.S., Collerson, K.D., 2000. Zr/Nb systematics of ocean island basalts reassessed: the case for binary mixing. Journal of Petrology 41, 1007–1021.

Kaymakçi, N., Aldanmaz, E., Langereis, C.G., Spell, T.L., Gurer, O.F., Zanetti, K.A., submitted for publication. Constraints on the Late Miocene transcurrent tectonics of NW Turkey: evidence from paleomagnetism and $^{40}Ar/^{39}Ar$ dating of the alkaline rocks. Geological Magazine.

Kellogg, J.B., Jacobsen, S.B., O'Connell, R.J., 2002. Modeling the distribution of isotopic ratios in geochemical reservoirs. Earth and Planetary Science Letters 204, 183–202.

Kinzler, R.J., 1997. Melting of mantle peridotite at pressures approaching the spinel to garnet transition: application to mid-ocean ridge basalt petrogenesis. Journal of Geophysical Research 102, 853–874.

Kogiso, T., Hirose, K., Takahashi, E., 1998. Melting experiments on homogeneous mixtures of peridotite and basalt: applications to the genesis of ocean island basalts. Earth and Planetary Science Letters 162, 45–61.

Kogiso, T., Hirschman, M.M., Reiners, P.W., 2004. Large scales of mantle heterogeneity and their relationship to ocean island basalt geochemistry. Geochimica et Cosmochimica Acta 68, 345–360.

Langmuir, C.H., Klein, E.M., Plank, T., 1992. Petrological systematics of mid-ocean ridge basalts: constraints on melt generation beneath ocean ridges. In: Phipps Morgan, J., Blackman, D.K., Sinton, J.M. (Eds.), Mantle Flow and Melt Generation at Mid-ocean Ridges, Geophys. Monogr., vol. 71. American Geophysical Union, pp. 183–280.

Lassiter, J.C., Hauri, E.H., Reiners, P.W., Garcia, M.O., 2000. Generation of Hawaiian post-erosional lavas by melting of a mixed lherzolite/pyroxenite source. Earth and Planetary Science Letters 178, 269–284.

LaTourette, T., Hervig, R.L., Holloway, J.R., 1995. Trace element partitioning between amphibole, phlogopite, and basanite melt. Earth and Planetary Science Letters 135, 13–30.

Le Bas, M.J., Le Maitre, R.W., Streckeisen, A., Zanettin, B., 1986. A chemical classification of volcanic rocks based on the total alkali–silica diagram. Journal of Petrology 27, 445–450.

Lundstrom, C.C., Hoernle, K., Gill, J., 2003. U-series disequilibria in volcanic rocks from the Canary Islands: plume versus lithospheric melting. Geochimica et Cosmochimica Acta 67, 4153–4177.

Maaløe, S., 1994. Estimation of the degree of partial melting using concentration ratios. Geochimica et Cosmochimica Acta 58, 2519–2525.

McDonough, W.F., Sun, S.-s., 1995. The composition of the earth. Chemical Geology 120, 223–253.

McKenzie, D.P., Bickle, M.J., 1988. The volume and composition of melt generated by extension of the lithosphere. Journal of Petrology 29, 627–679.

McKenzie, D.P., O'Nions, R.K., 1991. Partial melt distribution from inversion of rare earth element concentrations. Journal of Petrology 32, 1021–1991.

McKenzie, D.P., O'Nions, R.K., 1995. The source regions of ocean island basalts. Journal of Petrology 36, 133–159.

Niida, K., Green, D.H., 1999. Stability and geochemical composition of pargasitic amphibole in MORB pyrolite under upper mantle conditions. Contributions to Mineralogy and Petrology 135, 18–40.

Niu, Y., Bidaeu, D., Hèkinian, R., Batiza, R., 2001. Mantle compositional control on the extent of mantle melting, crust production, gravity anomaly, ridge morphology, and ridge segmentation: a case study at the mid-Atlantic ridge 33–35°N. Earth and Planetary Science Letters 186, 383–399.

Ozawa, K., 2001. Mass balance equations for open magmatic systems: trace element behavior and its application to open system melting in the upper mantle. Journal of Geophysical Research 106, 13407–13434.

Paton, S.M., 1992. The relationship between extension and volcanism in western Turkey, the Aegean Sea and Central Greece. Unpublished PhD Thesis, Cambridge University.

Pfister, M., Rybach, L., Şimsek, Ş., 1998. Geothermal reconnaissance of the Sea of Marmara region (NW Turkey): surface heat flow density in the area of active continental extension. Tectonophysics 291, 77–89.

Phipps Morgan, J., 1999. Isotope topology of individual hotspot basalt arrays: mixing curves or melt extraction trajectories? Geochemistry Geophysics Geosystems 1 (paper number 1999GC000004).

Pin, C., Briot, D., Bassin, C., Poitrasson, F., 1994. Concomitant separation of strontium and samarium–neodymium for isotopic analysis in silicate samples based on specific extraction chromatography. Analytica Chimica Acta 298, 209–217.

Roeder, P.L., Emslie, R.F., 1970. Olivine–liquid equilibrium. Contributions to Mineralogy and Petrology 29, 275–289.

Sato, K., Katsura, T., Ito, E., 1997. Phase relations of natural phlogopite with and without enstatite up to 8 GPa: implications for mantle metasomatism. Earth and Planetary Science Letters 146, 511–526.

Shaw, D.M., 1970. Trace element fractionation during anatexis. Geochimica et Cosmochimica Acta 34, 237–243.

Sun, S.-s., McDonough, W.F., 1989. Chemical and isotopic systematics of oceanic basalts: implications for mantle composition and processes. In: Saunders, A.D., Norry, M.J. (Eds.), Magmatism in the Ocean Basins, Special Publication, vol. 42. Geological Society of London, pp. 313–345.

Takazawa, E., Fred, F.A., Shimizu, N., Obata, M., Bodinier, J.-L., 1992. Geochemical evidence for melt migration and reaction in the upper mantle. Nature 359, 55–58.

van Keken, P.E., Hauri, E.H., Ballentine, C.J., 2002. Mantle mixing: the generation, preservation, and destruction of chemical heterogeneity. Annual Review of Earth and Planetary Sciences 30, 493–525.

Walter, M.J., 1998. Melting of garnet peridotite and the origin of komatiite and depleted lithosphere. Journal of Petrology 39, 29–60.

White, R.S., McKenzie, D.P., 1989. Magmatism at rift zones: the generation of volcanic continental margins and flood basalts. Journal of Geophysical Research 94, 7685–7729.

Wilson, M., Downes, H., Cebria, J.M., 1995. Contrasting fractionation trends in coexisting continental alkaline magma series; Cantal, Massif Central, France. Journal of Petrology 36, 1729–1753.

Yilmaz, Y., Polat, A., 1998. Geology and evolution of the Thrace volcanism, Turkey. Acta Vulcanologica 10, 293–303.

Zindler, A., Hart, S., 1986. Chemical geodynamics. Annual Review of Earth and Planetary Sciences 14, 493–571.

Zou, H.B., 1998. Trace element fractionation during modal and non-modal dynamic melting and open-system melting: a mathematical treatment. Geochimica et Cosmochimica Acta 62, 1937–1945.